

Response to Reviewers

We would like to thank the three reviewers for careful reading, insightful and constructive comments and helpful suggestions for our study. All comments have been addressed in the revised manuscript. We answer point by point to the comments and suggestions below. Reviewers' comments are included below in black font colour and our replies in blue. The revised and clarifying figures are included at the end of this document.

Reviewer 1:

General comments

This study investigates the lower tropospheric forcing of the major sudden stratospheric warming (MSSW), taking place in February 2018, and its predictability, using S2S database of the ECMWF. The main focus lies on two points: i) under which tropospheric conditions or forcings does the major warming occur (with a focus on the amplification of wave two in the stratosphere)?, and ii) why do some forecasts fail to predict the warming (within a time period of ± 1 day)? Two clusters are formed emphasizing the different evolution of the polar vortex within the forecast period. MSSW 2018 occurred under an amplification of planetary wave 2 which is mainly connected with anticyclones over Alaska and the Ural Mountains. A connection is drawn to the strong MJO phase 6 roughly two weeks before the onset. The anticyclone over the Ural mountains evolves and maintains under the forcing of wave trains modified by the strong MJO phase. This scale interaction starting to diverge within the ensemble over the North Atlantic sector. It is suggested that the missing MJO response towards the Northern Hemisphere and the modification of the synoptic scale wave trains is likely the cause. The paper is well written and clearly structured. It is the starting point to investigate which kind of processes belong to a systematic model bias and which are due to internal variability putting forward the S2S prediction system. Therefore I think the paper is worth for publishing after the authors have addressed the specific points below.

Specific comments

Data and Methods

- Which resolution (spatial and temporal) is used for the ECMWF ensemble forecast?

The horizontal resolution used for the ECMWF ensemble forecast is $1^\circ \times 1^\circ$ and the temporal resolution is 12 hours. We added information about the resolution to the Data and Methods section.

- Were the data evaluated on 12-hourly basis or daily mean basis?

The data were evaluated on the 12-hourly basis. We added this to the Data and Methods section.

- Geopotential height anomalies are calculated with respect to different time periods for ERA-Interim (1980-2010) and forecast ensemble (hindcasts: 1997-2017). Could we expect different anomalies only due to the different time periods? Have trends been removed?

We used the period of 1980-2010 as the longer the period is useful for cancelling the noise. However, in order to address this comment, we calculated ERA-Interim geopotential height anomalies with respect for the same time period as for the forecast ensemble: 1997-2017. We also removed trends in both datasets. The results show that the anomalies fields do not differ qualitatively due to the different time periods and detrending and our choices do not influence our conclusions (Figure AC1).

- Wave activity flux calculations can be used for different time scales spanning from e.g. 10 years down to 5-day mean averages. The investigated "quasi-stationary waves" changes under different temporal averaging. Which kind of temporal averaging is used for defining the prime quantities in the WAF calculations?

Wave activity flux (WAF) vectors can be indeed applied for different time scales, but due to the fast development of the SSW2018 we are using 3-day averages in the calculation of the Plumb flux. The Plumb (1985) formulation of the wave activity flux was used to study the SSWs occurred in 2009 (Harada et al., 2010) and in 2013 (Coy and Pawson, 2015) to identify the source regions and propagation of the wave activity.

Another formulation of WAF by Takaya and Nakamura (2001) given for zonally varying basic flow which can be used for illustrating an instantaneous status of the three dimensional wave propagation gives similar results to the Plumb WAF (Figure AC2). Both fluxes fields show good agreement in our case. We have updated the manuscript using the Takaya and Nakamura (2001) approach in the revised version.

- The MJO phase space is obtained by an EOF analysis of the combined fields. Long time scales should be filtered out before the index is calculated. Is a temporal filter applied to the

forecast data for calculating the MJO index based on anomalies? Is it necessary for 46-day forecasts?

The indexes were calculated at ECMWF using the Wheeler and Hendon (2004) method. According to this method the influence of seasonal cycle and interannual variability is removed before calculating the EOFs. The RMM indexes forecasted by the ECMWF extended-range prediction system can be obtained from the Subseasonal-to-Seasonal Prediction Project: <http://s2sprediction.net/>. This information is added to manuscript.

Stratospheric forecasts

- line 141: The fluctuations of the easterlies after the MSSW onset are very interesting. Are these fluctuations a result of the vacillation cycles (Holton and Mass, 1976)? The ensemble members do not capture these vacillations? Is the tropospheric forcing maybe not steady within the ensemble in contrast to ERA-In?

According to Holton and Mass (1976) large-scale stratospheric motions may vacillate in the irregular manner even with steady tropospheric forcing. However, the amplitude of this forcing plays the key role and defines if the oscillations in stratosphere are damped or not. Both period and amplitude of the stratospheric oscillations depend greatly on the strength of the initial forcing. In the SSW2018 case the oscillation period is approximately 4-6 days in ERA-I. The nature of these fluctuations is not clear to us, however we do not think that they are related to the Holton and Mass (1976) oscillations as the observed oscillations are too short to be associated with the Holton and Mass (1976) vacillations. Figure 2 from Holton and Mass (1976) suggests approximately 40-60 days cycle, depending on the amplitude of the tropospheric forcing. Period of these oscillations should be comparable to the period of radiation recovery in the lower stratosphere which controls the wave propagation, ca. 20 days. The fluctuations of zonal mean zonal wind in February 2018 might be induced by the horizontal propagation of waves and is likely connected to the vortex movement. Although the analysis of the vacillations of the easterlies after the SSW2018 onset in the re-analysis and forecast data seems to be an interesting topic it lies beyond the scope of our present paper.

- line 199-203: Figure 5 shows forecast spread at 50 hPa? Why is 50 hPa selected instead of 10 hPa (Figures before)?

We thank the reviewer for pointing that out and have changed the level in the Figure 5 to 10 hPa for consistency reasons. (Figure AC3). The geographical distribution of spread remains similar on both levels.

- Fig. 5 and Fig.6 show ensemble spread at 50 hPa and as a cross section at 50°N, respectively. The ensemble spread is in Fig.5c above 0.3 at 50°N at 50 hPa. Why is this not visible in Fig.6c? In Figure 6 of the manuscript the spread and anomaly are normalized by pressure, i.e. are multiplied by $(p/1000 \text{ hPa})$ and its square root respectively, for display reasons to facilitate the comparison across the different pressure levels. In Figure AC4 we show the spread that is not normalized by pressure and we also update this figure in the manuscript. We believe that there is no disagreement with Fig. 5c of the manuscript.

- In Fig. 6 the ensemble spread is gradually decreasing with height and remains below 0.1 above 150 hPa for the selected 3 dates. Why is the ensemble spread decreasing with height and remains low even if the forecast time proceeds?

In Figure 6 spread was normalized by pressure for display reasons. Here we include the figure for non-normalized spread and we also update this figure in the manuscript (Figure AC4). The spread is also normalized by the minimum and maximum values within the domain north of 20° N for each day separately to highlight the geographical spread rather than its growth with time.

Tropospheric waves

- Figure 9 shows the temporal evolution of the geopotential height at 250 hPa and the squared meridional wind component at the same level. Would a Hovmöller plot of the squared meridional wind component averaged between 40°N-65°N enhance the visibility of the wave trains (like e.g. Glatt et al., 2011)? The usage of the square of anomalous meridional wind provides an alternative (e.g. Chang, 1993).

In order to account for this comment, we plot a Hovmöller diagram of the squared meridional wind averaged over 40°N-65°N (Figure AC5). However, we do not find it more clear for tracking the wave trains in our case. In the manuscript we use the Nishii and Nakamura (2010) approach for highlighting the wave trains.

- The description of the coloured lines or coloured rectangles are missing in the captions of Figure 9 and Figure 10. A possible connection can be drawn in the paragraph starting at line 250. Is the contour interval in Fig.10 a,b the same as in Fig.9b?

The description of the colored lines is added to the captions (Figure AC6 and AC7) and mentioned in text as suggested. The contour intervals in Figures AC6b and AC7 a, b (Figures 9b and 10 a,b in manuscript, respectively) are the same: $800 \text{ m}^2 \text{ s}^{-2}$ (contour intervals are added to the figures captions).

technical corrections

- line 94: please, remove blank after "forecast"

Removed

Reviewer 2:

General comments

This study by Statnaia et al. examines the predictability of the February 2018 SSW by investigating the tropospheric conditions prior to the onset using the 51-member ensemble forecast of the ECMWF. In particular they focus on the role of tropospheric wave activity in the 10-14 days before the observed SSW date. They find that the Ural High region is particularly important for the onset of this SSW via the development of a blocking anticyclone in agreement with a recent study. This anticyclone was contributed to by the MJO phase 6-7, although this latter section is somewhat speculative in its nature. The paper is mostly well-written, although the English could do with some improvement (there are many places where the wrong article ['a' or 'the'] are used). Overall I find the paper quite interesting and thus warrants publication in WCD. My comments are all rather minor and hence my recommendation is publication with minor revisions.

Specific comments

Lines 95-98; to clarify, you only use forecasts that are initialized on 1st February? Have you examined any forecasts initialized before (and also after) this? If so, can you say something about them? How poor was the prediction skill of such forecasts? What is the 'fraction' mentioned in the two cited papers?

We thank the reviewer for this question. We focus in this study only on the forecast initialized on 1 February, because it is the first date when the forecast substantially changes from not showing the mean zonal wind reversal (Lee et al., 2019) to 14 ensemble members out of 51 predicting the reversal within 1 day from the observed onset date (Figure 1 of our manuscript). The ECMWF ensemble forecast is produced only twice a week (Monday and Thursday) and according to the forecast initialized on the 29 January no members showed reversal to easterlies (Lee et al., 2019). But the odds of an SSW in the forecast initialized on the 1 February increased by 2.5 times compared to the climatological frequency of easterlies on any February day which is 0.11 (Karpechko et al., 2018). On the other hand, with the reduction of the lead time the prediction skill increases rapidly and on 5 February the ensemble mean predict the negative zonal mean zonal wind (Karpechko et al., 2018). In order to investigate the driving mechanisms of the SSW2018 but not predictability as a function of lead time we focus on the first forecast showing the abrupt change to predicting the possibility of the event.

Line 116; 1) ‘used to localize regions on wave activity sources and sinks’ -> ‘...is used to identify localized regions of wave-activity sources and sinks.’ 2) In this diagnostic did you calculate for stationary waves? i.e., did you average the u,v,T etc in time prior to calculating the deviations from the zonal mean? Such a calculation is important as this diagnostic is only suitable for stationary waves. For transient waves, as is more appropriate here for synoptic-scale features, the flux of Takaya and Nakamura (2001) would be more apt.

1) Thank you, we corrected the sentence.

2) Thank you for pointing this out, we averaged all the parameters as 3-day mean and used the 5-7 February fields for analysis. But as the other reviewers also pointed out the more appropriate use of the Takaya and Nakamura (2001) flux, we show it here as well (Figure AC2). Both fluxes fields show good agreement in our case. We have updated the manuscript using the Takaya and Nakamura (2001) approach in the revised version.

Line 162; how many ensemble members actually maintained the easterlies for the period that ERAI shows?

Only 2 ensemble members maintained the easterlies until the end of February and returned to westerlies within 2 days from the observed reversal. This information is added to the manuscript.

Line 165; are these GPH anomalies that are shown? In section 2 you mention that GPH is only shown as anomalies, although this figure does not make it clear. Further on lone 167, you mention the 4-6th February GPH fields but they are not shown in figure 3. It would be useful to include them or at least state that they are not shown if that is the case.

We thank the reviewer for pointing this out. In Figure 3 the full geopotential fields are shown and we corrected this in Section 2 Data and Methods. We do not show the 4-6 February fields for space sake and we now mention this in text.

Lines 188-190; Such a relationship between wave1 and wave2 with one increasing and the other decreasing in amplitudes suggests some kind of wave-wave interaction occurring, i.e., wave2 grows at the expense of wave1 and vice versa. To diagnose this would be beyond the scope of this paper as it involves the enstrophy budget. However, a sentence on this may be useful as well as a suitable reference such as Smith (1983).

We agree with the reviewer about this point and therefore we have added the following sentence to the manuscript: “Moreover, the amplitude vacillation between PW1 and PW2 may be caused by wave-wave interactions (Smith, 1983).”

Line 199; What exactly is the ensemble spread shown here? The difference between the max and min ensemble members? i.e., the best and worst ensemble members? Or between the EN+ and EN- groups?

In Figures 5 and 6 of the manuscript we show the ensemble spread in geopotential height which is a measure of the difference between the members and is represented by the standard deviation with respect to the ensemble mean:

$$Spread = \frac{\sqrt{\frac{1}{N} \sum_{i=1}^N (g_i - \bar{g})^2}}{\bar{g}} \quad (1)$$

where g_i is geopotential height of an ensemble member, \bar{g} – ensemble mean, N – number of ensemble members (N=51).

We use the spread to assess the uncertainty in the forecast as small spread indicates high theoretical forecast accuracy, while large spread indicates low theoretical forecast accuracy. We have added the description of the ensemble spread to the Data and Methods section.

Figure 6; The contours are too dense to be able to make out the values of the spread shown by the shading, especially in panel a. Can you decrease the number of contours in all panels?

We have decreased the number of contours for a better visibility (Figure AC4 and Figure 6 in the manuscript).

Lines 227-228; I wonder if the Europe/Siberia sector can be considered as preconditioning the vortex prior to the reversal. Indeed, the North Atlantic sector appears to be the final straw with massive amplification just before the onset, but the Europe/Siberia sector is maximized a week or so before. Have you checked which wavenumbers dominate the flux in this figure? From figure 4 I would hazard a guess at wave-1, but it would be good to find out for sure.

We agree that the Siberian sector could have contributed to the preconditioning of the stratosphere during the period of wavenumber 1 amplification. Wave-1 is indeed dominating the stratosphere in about a week before the SSW onset in the Europe/Siberia sector (Fig. AC10). We have revised the manuscript to address this point and added the following to the text: “Additional analysis showed that wavenumber 2 was the largest contributor to the upward

wave activity during the week preceding SSW while wavenumber 1 was the largest contributor until 3-5 February (not shown), in agreement with wave amplitude evolution shown in Figure 4.”

Figure 9; what are the lines for? Presumably to show the blocking ridges and troughs. Please refer to them in the text and describe what they show in the caption; they could be useful in helping to explain to the reader. Further, figure 9b I find hard to understand what is going on. The features described on lines 258-265 are very difficult to see and as such I am not sure that I would agree with their characterization. For instance, the maximums in v'^2 on Feb 6th and 7th centered at 0E are characterized as two different events, but they could well be the same event. The max in v'^2 that is 80deg further downstream is characterized as part of the red-box event, but I find it rather unlikely that the feature would have travelled 80deg in one day. I find panel a much more believable and to me provides the necessary information that I would want to know; I would consider removing panel b entirely or at least making it clearer in the text exactly how you are tracking the features.

We have reworked the figures to make them more clear (Figures AC6 and AC7). The coloured lines suggest the propagation of wave trains; in the revised manuscript we have added this to the figures captions and in text. We believe that maximum in v'^2 on 6 February corresponds to the cut-off anticyclone centred over northern Scandinavia that during the next day remerged with the main flow at 60°E to form a blocking anticyclone there. This event corresponds to the wave breaking episode studied also by Lee et. al. (2019). The v'^2 maximum on 7 February is located some 20 degrees south of that on 6 February; therefore, we believe it corresponds to another ridge that was amplifying and travelling across the Atlantic during 5–6 February. We hope that updated figures illustrate this more clear. We also hope that redrawing the red line and extending the figure to 75°N makes it clear that the mean speed of this wave train between 6 and 8 February is about 30°–40°/day which is not unrealistic for wave train propagation.

Figure 11; Can you include the u contours on this plot to show how the winds and wave propagation are related. Further, the panels of the composite EN+ and EN- would be helpful to see how overall, the best and worst ensemble members capture the horizontal wave propagation compared to ERAI.

Please see the ERA-I zonal wind contours in Figure AC8 below. We find that adding u-contours to the manuscript figure makes it too noisy and is not very informative.

We find the separate panels of the composite EN+ and EN- yield less information than the difference between them, because the differences between the two clusters are practically indiscernible in this case (Figure AC9). We believe that adding ENS+ is sufficient. We have also updated the manuscript using the Takaya and Nakamura (2001) approach in the revised version.

Figure A2; over how many days are these trajectories run?

The length of the ECMWF extended-range ensemble forecast is 46 days, but we have plotted the forecast data for 1–28 February and the observed indexes for 15 January – 28 February. We have added these time intervals to the figure caption.

Line 318; Why is the central date here cast as February 7th? The central date in ERAI was 12th February throughout the earlier manuscript. Is this chosen as the period before which the vortex started being displaced and then splitting?

We thank the reviewer for this correction and have changed the text in the following way: “Before the SSW2018 central date an active MJO in phases 6 and 7 with large amplitude prevailed in tropical Indian ocean and South China Sea” as the MJO in phases 6 and 7 took place from 27 January until 18 February.

Line 332 and 339; how sensitive are the results in figure 14 to different lag stages? Given the previous comment, this can be important. Why exactly are lags 5-9 days before February 7th chosen? Figure 14; it is somewhat unclear from the caption and text exactly what this figure is showing. The contours are the ‘climatological’ response to every MJO phase 6-7 event, delayed by 5-9 days, in the 20 years of data? Then the shading represents the GPH anomalies just for the period 5-7th February for this one SSW event? Hence if the shading projects onto the contours then one could say there is constructive interference? Please clarify.

The MJO phase 6 took place on 27–31 January, therefore the effect of this tropical phenomena should be studied in the extratropics with a time lag. The lag of 5–9 days used in our study roughly corresponds to the period in the early February when the tropospheric waves forced SSW2018 (Figure 9 in the manuscript). The results are quite robust to different lags however the lag of 5–9 days yield the clearest fingerprint. In Figure 14 the contours indeed show the climatological (1980–2010) response to MJO phase 6 with the chosen lag superimposed on the anomalies of geopotential height for 5–7 February 2018 (shading) for comparison. The juxtaposition of these two fields on the same plot highlights that, apart from some dissimilarity

in the positions and strength of the features, their overall structure is well captured by the model. The geopotential height anomalies for 5–7 February 2018 are calculated using hindcasts for the previous 20 years produced on-the-fly with the real-time forecasts (1997–2010) which represent the model’s own climatology. For consistency we also recalculated the ERA-I climatology using the same period as for the re-forecasts however this does not change the results significantly (Figure AC1). We have updated the text to make it clearer by specifying what features we are pointing out.

Line 361; I would say that the EN- composite actually captures the global pattern pretty well in ERAI and EN+. It is the difference over the Urals/East Asia that is most pronounced as the observed wave-2 pattern is instead a wave-1 via a connection of the ridges.

Indeed, the difference over the Urals with two anticyclones merged is the most pronounced and it seems to us to be crucial in the SSW2018 case. To highlight this we have rewritten the text in the following way: “On the contrary, the response in the EN– cluster shows a PW1 pattern with two highs in Alaska and Ural region merged together (Fig. 14c), which is consistent with the EN– forecasts not capturing the amplification of PW2 in the stratosphere (Fig. 4c).”

Summary; Please include references to figure numbers throughout.

Reference to figure numbers is included in text. Thank you.

Technical comments

Line 40; add ‘a’ before ‘negative phase of the...’

Added

Line 101; what does EN stand for here? It is a little confusing as it can be easily mixed up with the El Nino phase (indeed initially I thought that was what it meant until I got to figure 2). Can you use a more appropriate acronym?

We changed EN to ENS, which stands for ‘ensemble’. Thank you.

line 225; ‘third’ -> ‘sector’

Corrected

Line 255; ‘cost’ -> ‘coast’

Corrected

Line 397; The sentence starting ‘Here we also’ does not make sense written as it. Please change to make clear.

We have rewritten the sentence in the following way: “We also showed that the wave packet crucial for the Ural blocking is not captured by the ensemble members that failed to forecast SSW2018.”

Lines 413-414; Rewrite sentence as ‘the composite analysis provides evidence, albeit indecisive, that teleconnections...’

Rewritten as proposed, thank you.

References: Smith 1983, Observations of wave-wave interactions in the stratosphere. JAS.

Reviewer 3:

General comments

The present manuscript analyses the sudden stratospheric warming that took place in mid-February 2018 (SSW2018). In particular, the study focuses on the tropospheric forcing of this phenomenon by examining its predictability based on the ECMWF ensemble forecast of the S2S initiative. The SSW2018 is found to be preceded by an amplification of wavenumber 2 wave activity in the stratosphere that is linked to the occurrence of a blocking in the Ural Mountains region. The authors also investigate the role of the record-breaking Madden Julian Oscillation (MJO) phase 6 in triggering the SSW event. The results show that this phenomenon might help, although its influence does not seem to be decisive.

The manuscript is well-written and the analysis is interesting. Thus, my recommendation is publication after having performed some minor changes.

Specific comments

L42-43: I think the clearest example of the interdecadal variability of SSW is the 2000s decade when there was an SSW in almost every winter and the 1990s decade with a very low frequency of SSWs.

We thank the reviewer for pointing that out. We have updated the text in the following way: “SSWs occur approximately once every second winter; however, there is no regularity: during the 1990s-decade SSWs occurred only twice while in the 2000s they took place almost every winter. During the last decade the events occurred in 2013, 2018, 2019.”

L57: Please note that some studies such as de la Cámara et al (2019) have also shown that it is not always necessary to have an enhancement of tropospheric waves for the occurrence of an SSW.

We thank the reviewer for this comment and have added it to the text: “However, SSWs are not always preceded by anomalous tropospheric wave activity. Some recent studies point out that the lower stratosphere dynamics and vortex geometry play role in the SSW onset (De La Cámara et al., 2019).”

L70: This was also shown by Ayarzagüena et al. (2018).

We added the reference to Ayarzagüena et al., (2018) in text.

L110-112: Is the data detrended?

As detrending was also pointed out by another reviewer we removed trends in datasets. Results show that the detrended fields do not differ qualitatively (e.g. see Figure AC1).

L115-123: Instead of the wave activity flux by Plumb (1985), I would suggest using the wave activity flux by Takaya and Nakamura (2001). This flux is defined for the case of a zonally varying basic flow, which, I think, is more appropriate in this study. The basic state in the Northern Hemisphere in winter shows inhomogeneities that can modulate the propagation of Rossby wave packets. Takaya and Nakamura's flux only focuses on the wave activity associated with Rossby wave packets, as the wavy anomalies are considered to be embedded in the basic flow that includes the climatological planetary waves. Actually, this flux was used by different authors to study tropospheric forcing of SSWs such as the event of January 2006 (Nishii et al. 2009) or the SSWs of 2009 and 2010 (Ayarzagüena et al., 2011).

Thank you for pointing this out. As the other reviewers have also pointed out the more appropriate use of the Takaya and Nakamura (2001) flux, we show it here as well (Figure AC2). Both fluxes fields show good agreement in our case. For calculating the flux by Plumb (1985) we averaged all the parameters as 3-day mean to account for the stationary waves.

We have updated the manuscript using the Takaya and Nakamura (2001) approach in the revised version and added the panel for EN+ for comparison with the reanalysis (Figure AC2).

L147-157: This evolution of the polar night jet (PNJ) is typical of split-vortex SSWs (S SSWs) (Charlton and Polvani, 2007). Before these events, the PNJ typically shifts poleward and then, the vortex splits into two pieces. Albers and Birner (2014) also show that the polar vortex before S SSWs tends to be constrained around the pole and has little vertical tilt. I think some comment about that could be added.

We have added the following in the text: "The position of the vortex close to the pole and little vertical tilt are typical for the split SSWs as was pointed out by Albers and Birner (2014)."

L205-207 and figure 6: it is difficult for me to identify the regions with large ensemble forecast spread.

In Figure 6 spread and anomaly are normalized by pressure, i.e. are multiplied by $(p/1000 \text{ hPa})$ and its square root, respectively for display reasons. In Figure AC4 we show the spread that is not normalized by pressure and update the manuscript accordingly.

L217-229: I agree with the authors that there are some bursts of wave activity in the troposphere before the occurrence of SSW2018. I also agree on the enhancement of wave activity in the stratosphere, particularly in the North Atlantic sector. However, I have the impression that apart from the tropospheric forcing there is a self-amplification of the wave activity in the stratosphere. These results would be also consistent with the characteristics of wave activity during S SSWs highlighted by previous studies. For instance, Plumb (1981) and Albers and Birner (2014) indicate that it is typical for S SSWs that an initial vortex structure close to its resonant point can split the vortex with only a small increase in tropospheric wave forcing. I would suggest adding some comments about that in the text.

We added these results in the text: “Note that, enhanced tropospheric forcing, in addition to directly affecting the mean stratospheric circulation, may also alter the geometry of the vortex and precondition it to splitting by triggering the internal resonance (Albers and Birner, 2014).”

L241-245: When split into three regions, the correlation coefficient between the vertical component of the WAF forecasts on 4–11 February and U10 forecasts on 12 February is not statistically significant in the troposphere. Do you know why?

The reviewer raises a very interesting question, but we can only speculate about why the correlation coefficient is not significant in the troposphere which might lead to more confusion than clarity.

L257-265: I must confess I find it difficult to see the propagation of synoptic structures in Figure 9b. In this sense, I am not 100% sure that the anomalies of v^{250^2} on 8 February around 80°E are related to the anomalies over the Eastern Atlantic at the beginning of February, as the red box in figure 9b seems to indicate. There are already some anomalies at high latitudes in Eurasia on 6 February that seem to intensify in the following days. A similar evolution is detected in Figure 10a for EN+ members, but in EN- members you have a very similar pattern over the North Atlantic on 3-6 February, but the development of the anomalies over the Eurasia is missing.

We have reworked the figures to make them more clear (Figures AC6 and AC7). The coloured lines suggest propagation of wave trains, in the revised manuscript we have added this to the figures captions and in text. In particular we hope that extension of the plots up to 75°N shows the evolution of the red wave train clearer. We believe that the red wave train and subsequent wave breaking led to the formation of a zonally elongated cut-off anticyclone on 6 February which had v'^2 maximums on both flanks, around 0°E and 80°E . Note that this wave train

propagates at speed of 30° – 40° /day, which is reasonable. After 6 February, the left flank, as indicated by v'^2 maximum continues to move eastward while the right flank remains stationary and intensifies. This wave train finally contributed to the blocking anticyclone over Ural. This event corresponds to the wave breaking episode studied also by Lee et. al. (2019). We point out the missing development of the anomalies in EN– members in text as one of the most prominent differences between the two ensemble members groups.

L321: please add “the”

Added

L397: we have also shown

We have rewritten this sentence in the following way: “We have also shown that the wave packet crucial for the Ural blocking is not captured by the ensemble members that failed to forecast SSW2018.”

L397-399: please rewrite this sentence.

We have rewritten this sentence in the following way: “We have also shown that the wave packet crucial for the Ural blocking is not captured by the ensemble members that failed to forecast SSW2018.”

L419: Domeisen et al. 2019a or b?

Corrected: Domeisen et al., 2019a

Figure 14, caption: It is not 100% clear for me what you are showing in contours. Is it the geopotential height anomalies for all MJO phase 6 in the whole period of study? I understood so, but it would be great if you indicate it more clearly in the text.

We have rewritten the figure caption in the following way: “Geopotential height anomalies at 500 hPa in (a) ERA-I; (b) ENS+ members and (c) ENS– members. Contours show geopotential height composite (m) for MJO phase 6 averaged over lags 5–9 days. Shading shows anomalies averaged over 5-7 February 2018. ERA-I composites are calculated using 1980–2010 data. Forecast model composites are calculated using hindcasts over 1997–2017.”

We have also clarified this in text: “In Fig. 14a contours represent the composite fields showing the climatological ERA-I fingerprint of the MJO phase 6. Contours in Figures 14 b and c show similar fingerprint but constructed with the model hindcasts over the 20-years period.”

References:

- Albers, J. R. and Birner, T.: Vortex Preconditioning due to Planetary and Gravity Waves prior to Sudden Stratospheric Warmings, *J. Atmos. Sci.*, 71(11), 4028–4054, doi:10.1175/jas-d-14-0026.1, 2014.
- Ayarzagüena, B., Barriopedro, D., Garrido-Perez, J. M., Abalos, M., de la Cámara, A., García-Herrera, R., Calvo, N. and Ordóñez, C.: Stratospheric Connection to the Abrupt End of the 2016/2017 Iberian Drought, *Geophys. Res. Lett.*, 45(22), 12,639–12,646, doi:10.1029/2018GL079802, 2018.
- Coy, L. and Pawson, S.: The major stratospheric sudden warming of January 2013: Analyses and forecasts in the GEOS-5 data assimilation system, *Mon. Weather Rev.*, 143(2), 491–510, doi:10.1175/MWR-D-14-00023.1, 2015.
- Harada, Y., Goto, A., Hasegawa, H., Fujikawa, N., Naoe, H. and Hirooka, T.: A Major Stratospheric Sudden Warming Event in January 2009, *J. Atmos. Sci.*, 67(6), 2052–2069, doi:10.1175/2009jas3320.1, 2010.
- Holton, J. R. and Mass, C.: Stratospheric vascillation cycles, *J. Atmos. Sci.*, 33, 2218–2225 [online] Available from: [https://doi.org/10.1175/1520-0469\(1976\)033%3C2218:SVC%3E2.0.CO;2%0A](https://doi.org/10.1175/1520-0469(1976)033%3C2218:SVC%3E2.0.CO;2%0A), 1976.
- Karpechko, A. Y., Charlton-Perez, A., Balmaseda, M., Tyrrell, N. and Vitart, F.: Predicting Sudden Stratospheric Warming 2018 and Its Climate Impacts With a Multimodel Ensemble, *Geophys. Res. Lett.*, 45(24), 13,538–13,546, doi:10.1029/2018GL081091, 2018.
- De La Cámara, A., Birner, T. and Albers, J. R.: Are sudden stratospheric warmings preceded by anomalous tropospheric wave activity?, *J. Clim.*, 32(21), 7173–7189, doi:10.1175/JCLI-D-19-0269.1, 2019.
- Lee, S. H., Charlton-Perez, A. J., Furtado, J. C. and Woolnough, S. J.: Abrupt stratospheric vortex weakening associated with North Atlantic anticyclonic wave breaking, *J. Geophys. Res. Atmos.*, 2019JD030940, doi:10.1029/2019JD030940, 2019.
- Nishii, K. and Nakamura, H.: Three-dimensional evolution of ensemble forecast spread during the onset of a stratospheric sudden warming event in January 2006, *Q. J. R. Meteorol. Soc.*, 136(649), 894–905, doi:10.1002/qj.607, 2010.
- Plumb, R. A.: On the Three-Dimensional Propagation of Stationary Waves, *J. Atmos. Sci.*,

42(3), 217–229, doi:10.1175/1520-0469(1985)042<0217:ottdpo>2.0.co;2, 1985.

Smith, A. K.: Observation of Wave-Wave Interactions in the Stratosphere, *J. Atmos. Sci.*, 40, 2484–2496, doi:[https://doi.org/10.1175/1520-0469\(1983\)040<2484:OOWWII>2.0.CO;2](https://doi.org/10.1175/1520-0469(1983)040<2484:OOWWII>2.0.CO;2), 1983.

Takaya, K. and Nakamura, H.: A Formulation of a Phase-Independent Wave-Activity Flux for Stationary and Migratory Quasigeostrophic Eddies on a Zonally Varying Basic Flow, *J. Atmos. Sci.*, 58(6), 608–627, doi:10.1175/1520-0469(2001)058<0608:afopi>2.0.co;2, 2001.

Wheeler, M. C. and Hendon, H. H.: An All-Season Real-Time Multivariate MJO Index : Development of an Index for Monitoring and Prediction, *Mon. Weather Rev.*, 132, 1917–1932, 2004.

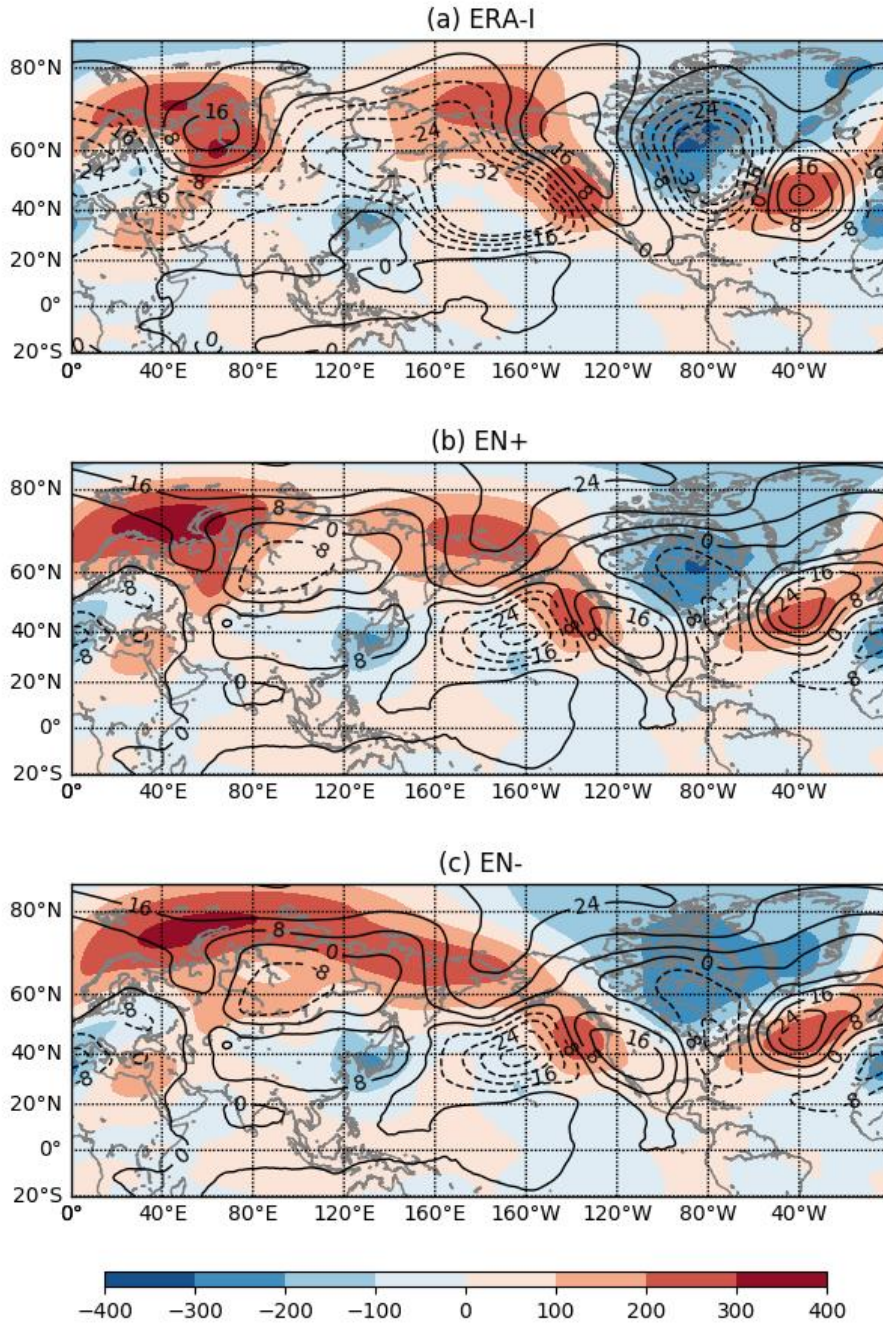


Figure AC1. Geopotential height anomalies at 500 hPa in (a) ERA-I; (b) ENS+ members and (c) ENS- members. Contours show geopotential height composite (m) for MJO phase 6 averaged over lags 5–9 days. Shading shows anomalies averaged over 5–7 February 2018. ERA-I composites are calculated using 1980–2010 data. Forecast model composites are calculated using hindcasts over 1997–2017.

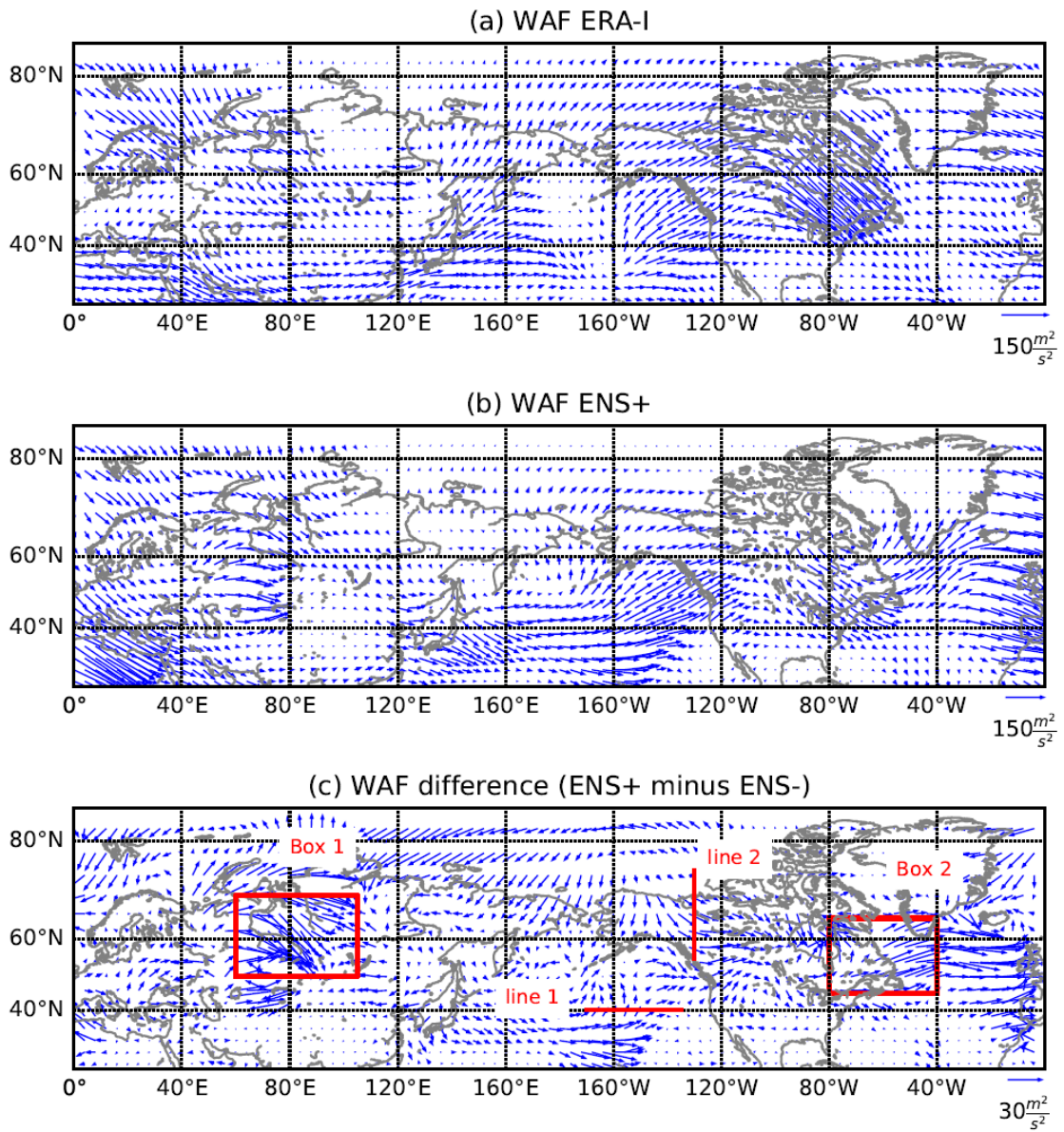


Figure AC2. The 500 hPa horizontal WAF calculated following Takaya and Nakamura (2001) ($m^2 s^{-2}$) averaged over 5–7 February. (a) ERA-Interim; (b) ENS+; (b) difference between EN+ and EN– groups of ensemble members.

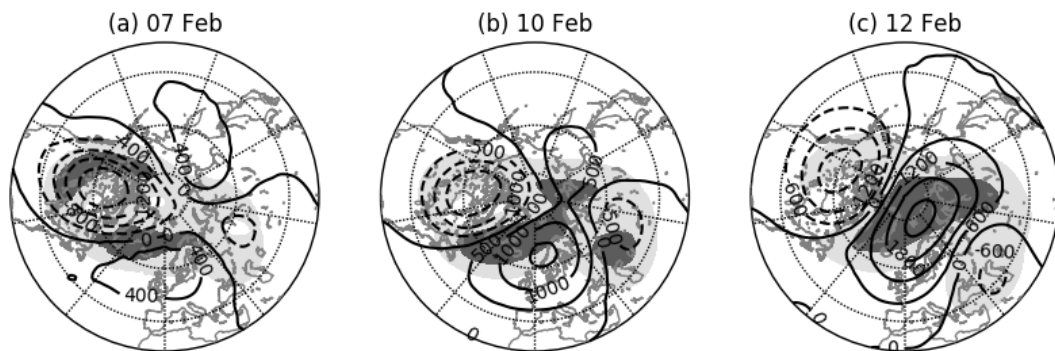


Figure AC3. ERA-I 10 hPa geopotential height anomalies (contours, m) with respect to the 1980–2010 climatology and ensemble spread of geopotential height predicted for (a) 7, (b) 10 and (c) 12 February 2018 (shaded lightly and heavily for 0.3–0.6 values and values greater than 0.6, respectively). The spread has been normalized by the minimum and maximum values within the domain north of 20° N.

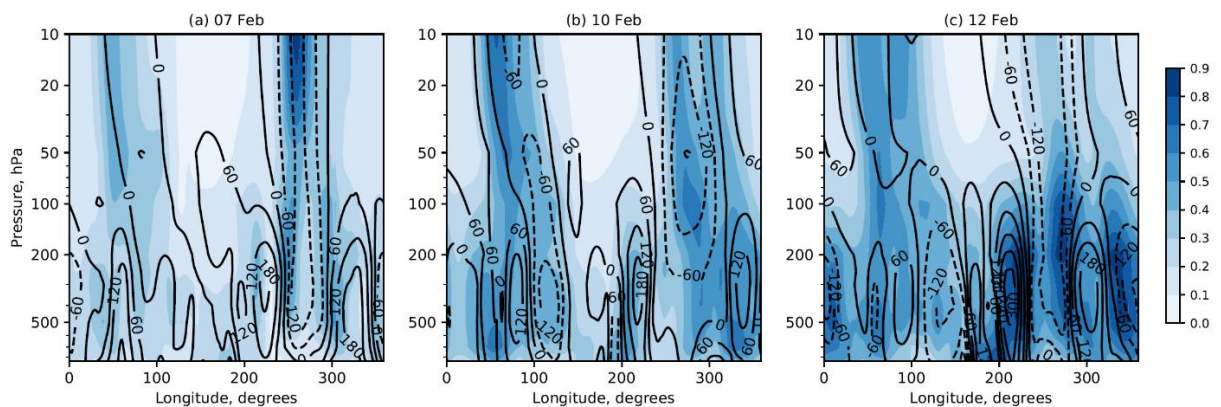


Figure AC4. Zonal cross-sections for 50° N of the ensemble spread of geopotential height predicted for (a) 7, (b) 10 and (c) 12 February 2018. Superimposed contours represent observed geopotential anomalies (m) with respect to the 1980–2010 climatology. Solid lines represent anticyclonic (positive) anomalies and dashed lines cyclonic (negative) anomalies. Anomaly is normalized by pressure.

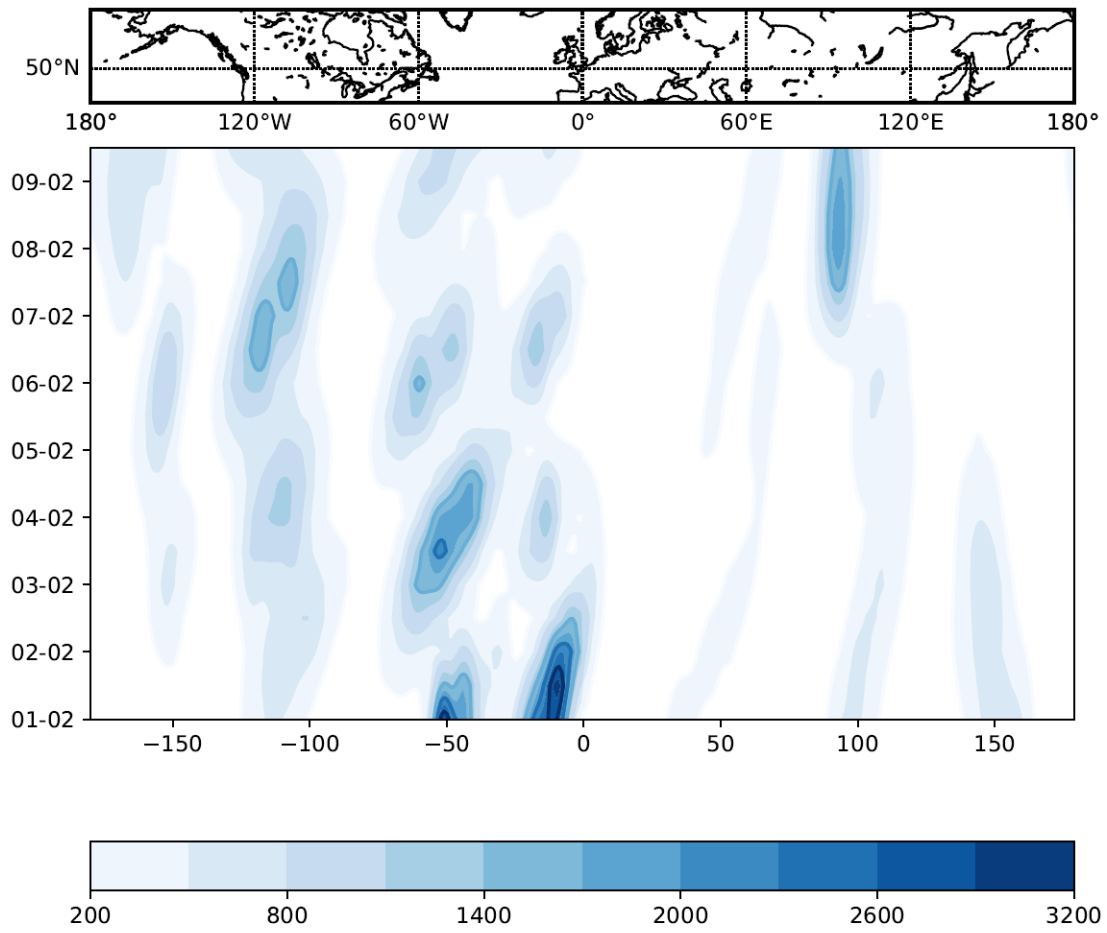


Figure AC5. Hovmöller diagram of the squared velocity of meridional wind (m^2/s^2) from 1 February 2018 until 9 February averaged over a latitudinal belt (40°N - 65°N) at 250hPa. Contours are smoothed with a Gaussian filter and start at $200 \text{ m}^2/\text{s}^2$ with an interval of $300 \text{ m}^2/\text{s}^2$. The map in the upper panel is given to indicate the latitudinal belt used for averaging and geographical reference.

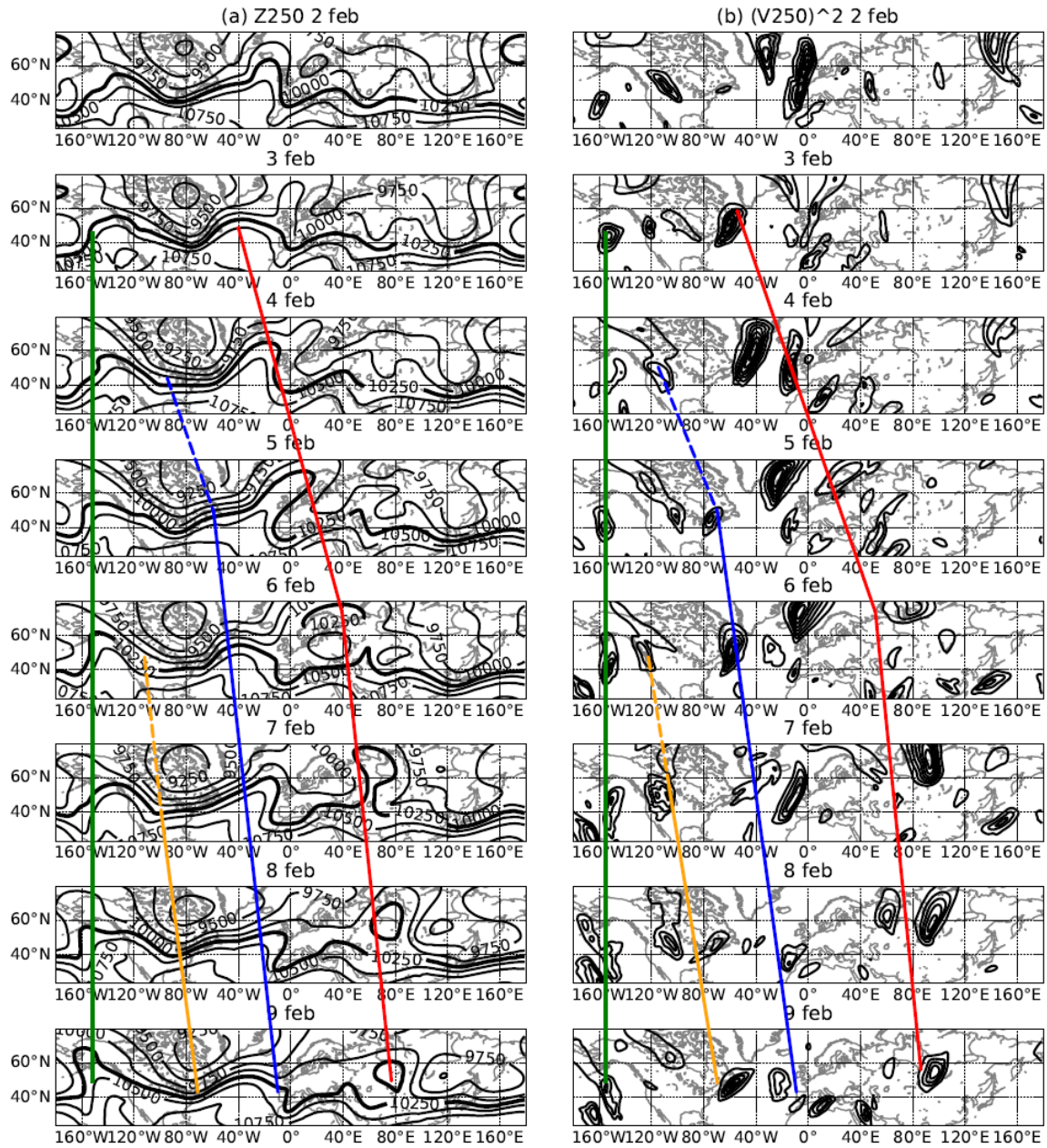


Figure AC6. Time sequence of (a) ERA-I 250 hPa geopotential height observed from 2 (top) to 9 (bottom) February 2018 over a domain (20° N–70° N). The thick contour corresponds to 10250 m. (b) ERA-I 250 hPa meridional velocity squared, contour intervals are 800 m² s⁻². The coloured lines track the movement of the ridges and troughs (a) and maximums of meridional velocity squared (b) and suggest the propagation of wave packets.

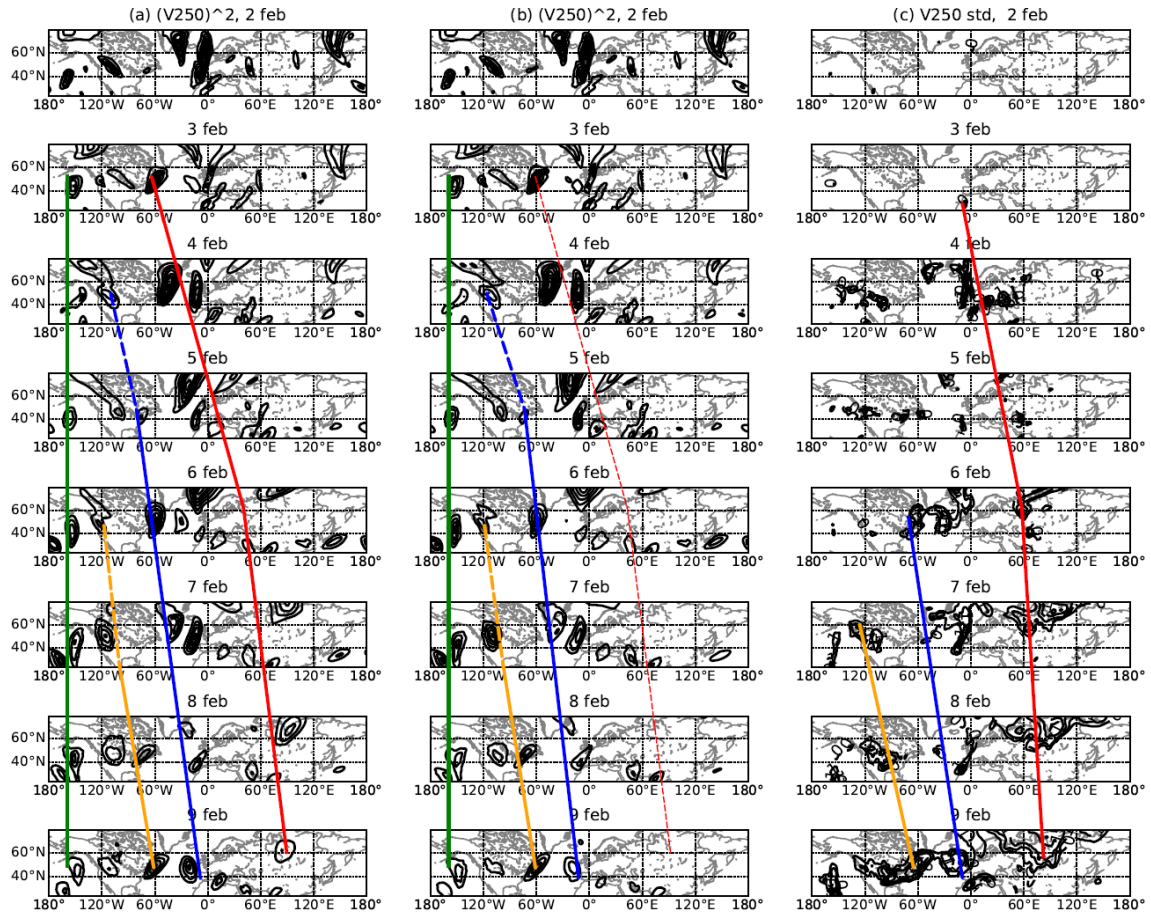


Figure AC7. Same as Fig. AC7b, but for EN+ (a) and EN- (b) members, contour intervals are $800 \text{ m}^2 \text{ s}^{-2}$; (c) standard deviation of the predicted 250 hPa meridional wind velocity among ensemble members. The standard deviation is normalized by the maximum and minimum within the domain. Contour intervals are 0.1 starting from 0.5. The coloured lines are mostly similar to those in Figure 9 and suggest the propagation of wave packets. The red line in Figure 10b is dashed to emphasize the lack of this wave train in ENS-. The green line in Figure 10c is missing because there is little forecast spread in the eastern Pacific.

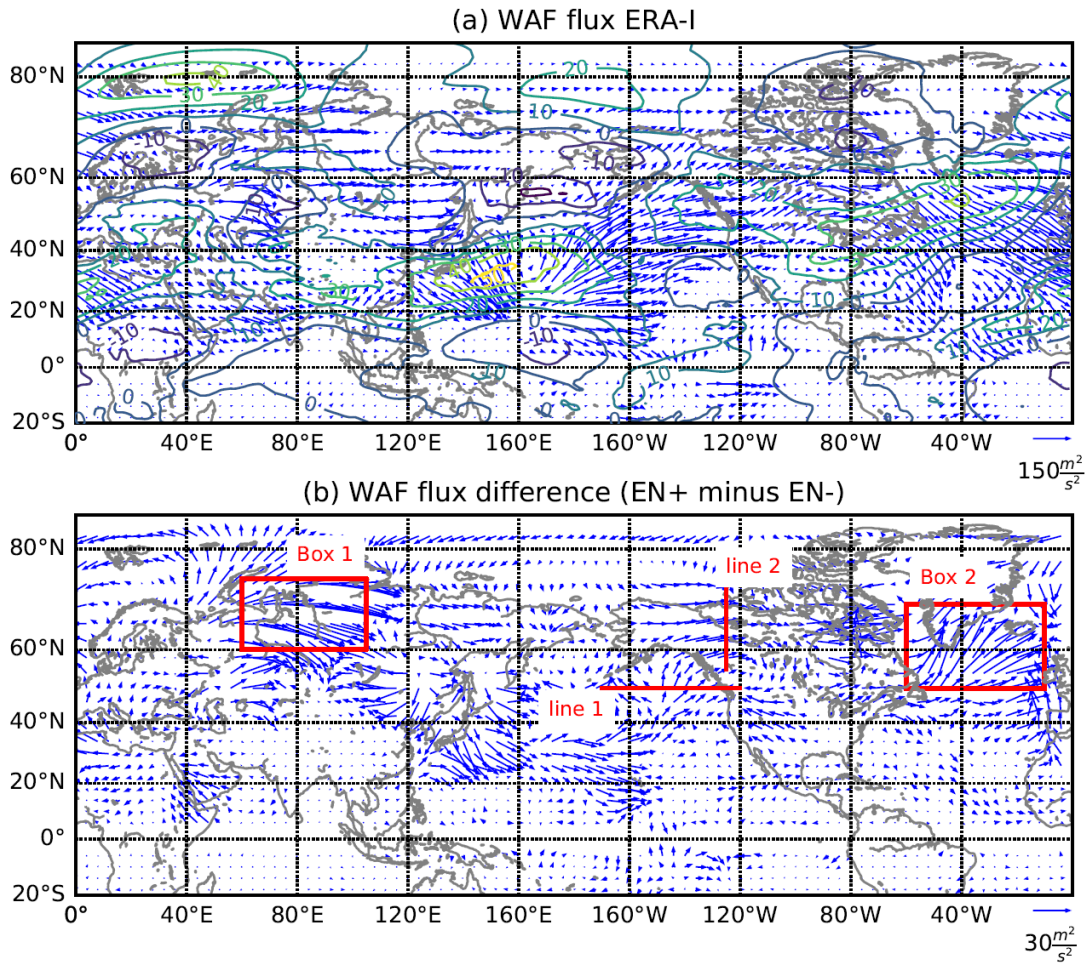


Figure AC8. The 500 hPa horizontal WAF (Plumb, 1985) ($\text{m}^2 \text{s}^{-2}$) averaged over 5–7 February. (a) ERA-Interim, contours show zonal wind; (b) difference between EN+ and EN– groups of ensemble members.

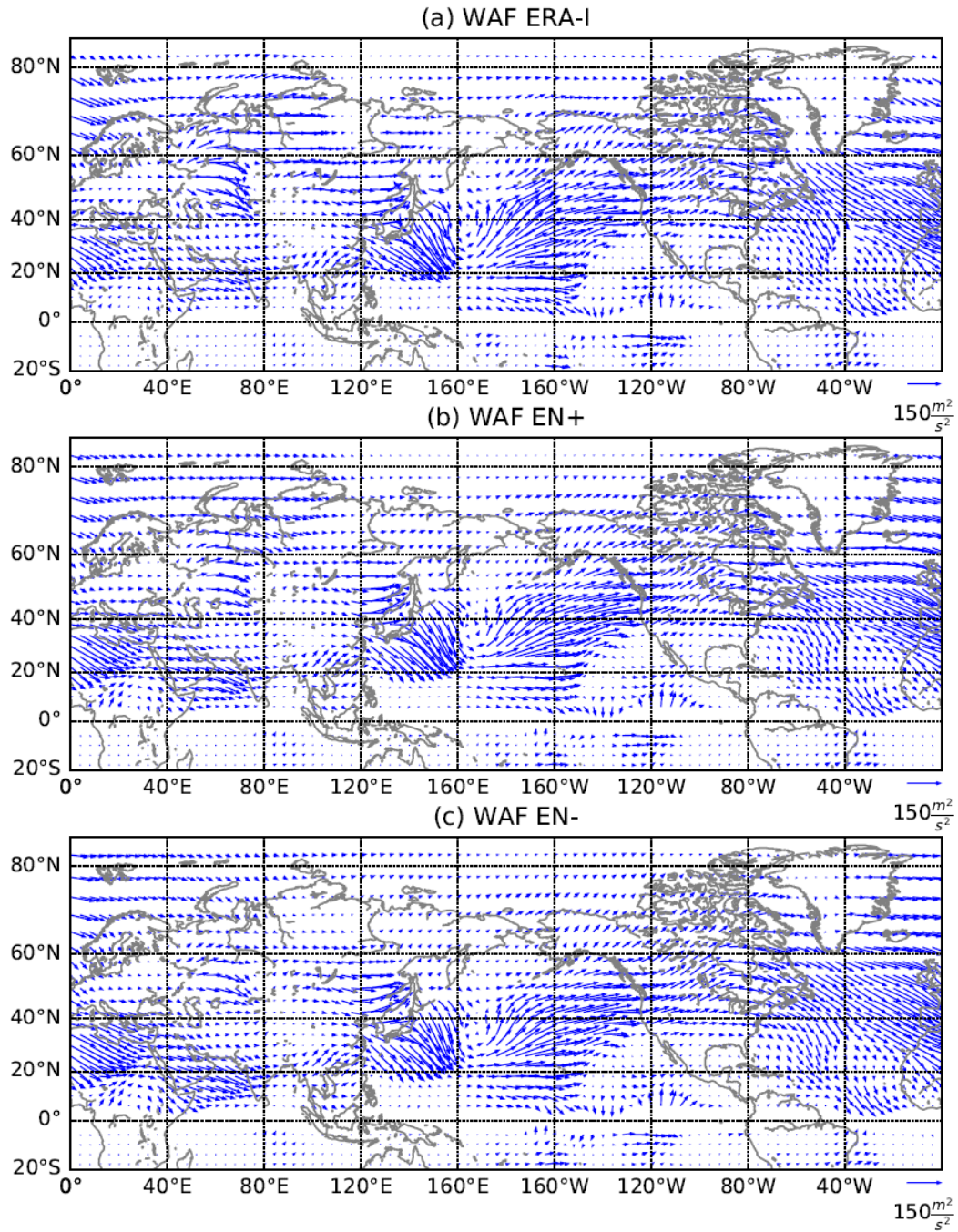


Figure AC9. The 500 hPa horizontal WAF (Plumb, 1985) ($m^2 s^{-2}$) averaged over 5–7 February. (a) ERA-Interim; (b) composite EN+ and (c) EN–.

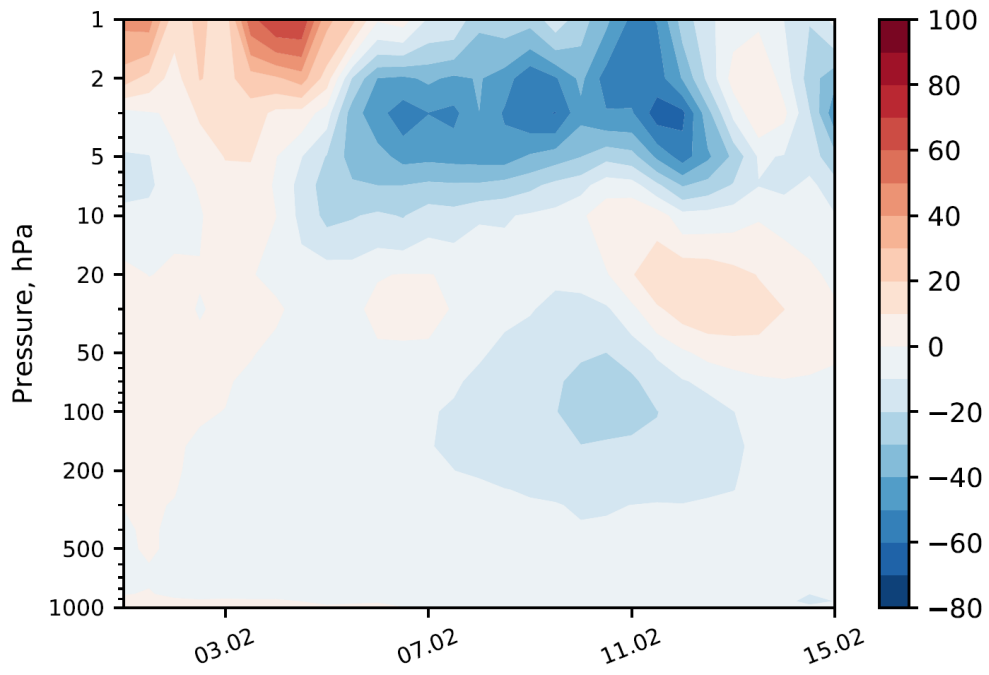


Figure AC10. Time-altitude plot of the heat flux $v'T'$ difference between waves 1 and 2 for the Europe/Siberia sector (0-120°E).

Mechanisms and predictability of Sudden Stratospheric Warming in winter 2018

Irina A. Statnaia^{1,2}, Alexey Yu. Karpechko¹, Heikki J. Järvinen²

¹Finnish Meteorological Institute, 00560 Helsinki, Finland

5 ²Institute for Atmospheric and Earth System Research, Faculty of Science, University of Helsinki, 00014 Helsinki, Finland

Correspondence: Irina A. Statnaia (irina.statnaia@helsinki.fi)

Abstract. In the beginning of February 2018 a rapid deceleration of the westerly circulation in the polar Northern Hemisphere stratosphere took place and on 12 February the zonal mean zonal wind at 60° N and 10 hPa reversed to easterly in a Sudden Stratospheric Warming (SSW) event. We investigate the role of the tropospheric forcing in the occurrence of the SSW, its predictability and teleconnection with the Madden-Julian oscillation (MJO) by analysing the European Centre for Medium-Range Weather Forecasts (ECMWF) ensemble forecast. The SSW was preceded by significant synoptic wave activity over the Pacific and Atlantic basins, which led to the upward propagation of wave packets and resulted in the amplification of a stratospheric wavenumber 2 planetary wave. The dynamical and statistical analyses indicate that the main tropospheric forcing resulted from an anticyclonic Rossby wave breaking, subsequent blocking and upward wave propagation in the Ural Mountains region, in agreement with some previous studies. The ensemble members which predicted the wind reversal, also reasonably reproduced this chain of events, from the horizontal propagation of individual wave packets to upward wave activity fluxes and the amplification of wavenumber 2. On the other hand, the ensemble members which failed to predict the wind reversal, also failed to properly capture the blocking event in the key region of the Urals and the associated intensification of upward propagating wave activity. Finally, a composite analysis suggests that teleconnections associated with the record-breaking MJO phase 6 observed in the late January 2018 likely played a role in triggering this SSW event.

1 Introduction

Sudden stratospheric warmings (SSWs) are the most prominent phenomena taking place in the wintertime polar stratosphere and representing the dynamical linkage between troposphere and stratosphere. During a major SSW event the zonal mean zonal winds at 10 hPa and 60° N reverse from westerlies to easterlies and the stratospheric temperature rises by several tens of Kelvins over the course of a few days (Butler et al., 2015). SSWs have been shown to be related to the enhancement of tropospheric forced planetary wave packets that propagate upward into the stratosphere and interact

with the mean flow (Charney and Drazin, 1961; Matsuno, 1971; McIntyre, 1982; Limpasuvan et al.,
35 2004). These upward propagating planetary waves amplify with height, approaching the critical level
where they irreversibly break and deposit westward angular momentum (quantified as a convergence
of the Eliassen-Palm flux), which leads to the deceleration and breaking down of the polar night jet
(Polvani and Saravanan, 2000). Stratospheric circulation anomalies, in turn, can influence the
troposphere (Kuroda and Kodera, 1999; Baldwin and Dunkerton, 1999). In particular, it can lead to
40 the development of [a negative phase of the Northern Annular Mode \(NAM\)](#), shifting tropospheric
storm tracks southward and making northern and central Europe prone to cold Arctic air masses
(Thompson et al., 2002). SSWs occur approximately once every second winter; however, there is no
regularity: [during the 1990s-decade SSWs occurred only twice while in the 2000s they took place
almost every winter](#). During the last decade the events occurred in 2013, 2018, 2019. The 2013 and
45 2018 events were followed by cold and snowy weather in Europe (Nath et al., 2016; Karpechko et
al., 2018). Since the stratosphere tends to be more predictable than the troposphere, SSWs are
considered to be a potential source of extended-range predictability (Christiansen, 2005; Sigmund et
al., 2013; Scaife et al., 2016; Karpechko, 2015; Domeisen, Butler, Charlton-Perez, et al., 2019; Kautz
et al., 2019). It is therefore important to understand factors controlling the variability of the polar
50 vortex and SSWs generation.

External forcings such as the quasi-biennial oscillation (QBO) (Holton and Tan, 1980), Madden-
Julian oscillation (MJO) (Garfinkel et al., 2012) or El Niño Southern Oscillation (ENSO) (Taguchi
and Hartmann, 2006; Song and Son, 2018) may ~~trigger~~ [shift the stratosphere towards](#) such anomalous
~~stratospheric~~ states as SSWs acting as a source of Rossby wave packets or influencing their vertical
55 propagation (Lu et al., 2012). It has been shown that some major SSWs have been preceded by
tropospheric blockings that modify tropospheric planetary waves in such a way that they can
influence the onset and type of an SSW (Nishii and Nakamura, 2004; Martius et al., 2009; Woollings
et al., 2010; Castanheira and Barriopedro, 2010; Quiroz, 1986). [However, SSWs are not always
preceded by anomalous tropospheric wave activity. Some recent studies point out that the lower
60 stratosphere dynamics and vortex geometry play an important role in the SSW onset](#) (De La Cámara
et al., 2019).

The onset and dynamical evolution of each SSW event is a combination of the typical
characteristics and its unique features, therefore detailed investigation of each case can advance our
understanding of large-scale processes in the boreal winter stratosphere and improve their prediction.
65 On 12 February 2018 a prominent vortex split type major SSW occurred (hereafter referred to as
SSW2018) (Karpechko et al., 2018; Lee et al., 2019). The split type events are considered to be less
predictable than the displacement events, especially at lead times of 1–2 weeks (Domeisen et al.,

2019). SSW2018 occurred under the favourable conditions of the easterly phase of QBO, La Niña phase of ENSO and followed the MJO phase 6 with the largest amplitude in observational record (from 1974 to 2018) (Barrett, 2019). Barrett (2019) showed that the large-amplitude MJO episode in 2018 affected weather in the north-eastern United States under the conditions of strengthened Rossby wave teleconnections between the tropics and the extratropics. Furthermore, SSW2018 was preceded by a record-breaking meridional eddy heat flux at 100 hPa observed before an SSW since 1958 (see Fig. A1 in Appendix A, [also pointed out by](#) (Ayarzagüena et al., (2018))).

In this study we investigate the role of the tropospheric forcing in SSW2018, its predictability and teleconnection with the MJO by analysing the European Centre for Medium-Range Weather Forecasts (ECMWF) ensemble forecast. The purpose of the paper is to present results of the analysis of the atmospheric circulation in the stratosphere and troposphere before and during SSW2018 and clarify the driving mechanisms focusing on the amplification of the upward wave activity propagation into the stratosphere before the SSW onset. Karpechko et al. (2018) showed that the lead time for the SSW2018 prediction varied among the 11 individual models of the subseasonal-to-seasonal (S2S) database of extended range forecasts. They suggested that the errors in the forecast location of an anticyclone over the Urals (the Ural high) played the crucial role in reducing the SSW2018 predictability. This result is being proved in the present study with additional analysis of the Ural high onset. The importance of wave breaking in the building of the Ural high and critical role of an Atlantic cyclogenesis was highlighted by Lee et al. (2019). On the other hand, Rao et al. (2018) pointed to the Alaskan blocking as the source of intensified extratropical wavenumber 2 planetary wave that was important for triggering SSW2018. In this paper we will extend the analysis of previous papers and present further evidence that several Rossby wave trains that developed in the troposphere and originated from localized quasi-stationary blocking highs have likely contributed to the SSW2018 forcing.

The paper is organized as follows. In Section 2 the data and analysis methods are briefly described. In Section 3 we present dynamical features of SSW2018 and contrast evolution of forecast ensemble members that predicted and did not predict SSW2018 at 11 days lead time. In particular, we present evidence that MJO teleconnection played a role in triggering SSW2018. In the final section we present our conclusions.

2 Data and Methods

This study is based on the ECMWF 46-day coupled ocean-atmosphere ensemble forecast-, produced twice a week (Monday and Thursday) with 51 members (Vitart et al., 2017). [In this study we use the 12-hourly forecast data on a horizontal grid of 1°×1° resolution.](#) We chose the forecast initialized on

1 February 2018 to test the predictability of SSW2018 and analyse the error growth. The date is selected based on Karpechko et al. (2018) and Lee et al. (2019) who showed that this was the first forecast date when a considerable fraction of ensemble members predicted SSW2018. To discern the errors and their possible sources, we selected two groups of ensemble members for further analysis and comparison with the reanalysis fields:

- ENS+ cluster: 10 ensemble members which succeeded in forecasting the wind reversal at 10 hPa and 60° N within +/- 1 day from the observed onset date (12 February) (Fig. 1);
- ENS- cluster: 10 ensemble members which maintained the largest positive values of the zonal mean zonal wind at 10 hPa and 60° N across the ensemble members.

Hereafter, we analyse the composite fields of these two groups while all ensemble members are used to illustrate forecast spread and correlations for several diagnostics.

For the forecast verification, we use the ECMWF ERA-Interim reanalysis (ERA-I, Dee et al., 2011). The present analysis includes the period from 1979 to 2018. 12-hourly data are used on a 1°×1° horizontal grid covering the Northern Hemisphere (NH).

Stratospheric wind, eddy heat flux and wave activity flux are analysed as full fields while geopotential height is analysed as an anomaly except for the Fig. 3. ERA-I anomalies are calculated with respect to the period 1980–2010. The forecast anomalies are defined as the subtraction of the model's own climatology from the forecast fields. Model's own climatology is computed using hindcasts over the prior 20 years: 1997–2017. We tested that our results do not change significantly if we calculate ERA-I climatology over the same period as that in the forecast model or if we detrend the fields before calculating anomalies; and thus, our choices do not affect the conclusions.

We use the ensemble spread to assess the uncertainty in the forecast as small spread indicates high theoretical forecast accuracy, while large spread indicates low theoretical forecast accuracy. We show the ensemble spread in geopotential height which is a measure of the difference between the members and is represented by the standard deviation with respect to the ensemble mean:

$$Spread = \frac{\sqrt{\frac{1}{N} \sum_{i=1}^N (g_i - \bar{g})^2}}{\bar{g}} \quad (1)$$

where g_i is geopotential height of an ensemble member, \bar{g} – ensemble mean, N – number of ensemble members (N=51).

The wave activity flux (WAF) ~~that~~ indicates a propagating packet of planetary waves in the three-dimensional space and is used to identify localized regions of wave-activity sources and sinks ~~can be used to localize regions on wave activity sources and sinks~~. Here we use the WAF defined for a

zonally varying basic flow following (Takaya and Nakamura, (2001)). Following Plumb (1985), wave activity flux \vec{F}_s on the sphere is represented in log-pressure coordinates as:

$$\vec{F}_s = \begin{pmatrix} F_x \\ F_y \\ F_z \end{pmatrix} = p \cos\varphi \begin{pmatrix} \frac{v'^2}{2\Omega a \sin 2\varphi} + \frac{\delta(v'\Phi')}{\delta\lambda} \\ u'v' + \frac{\delta(u'\Phi')}{2\Omega a \sin 2\varphi} \\ \frac{2\Omega \sin\varphi}{S} \left[v'T' + \frac{\delta(T'\Phi')}{2\Omega a \sin 2\varphi} \right] \end{pmatrix}, \quad (1)$$

135 where F_x, F_y, F_z denote the zonal, meridional and vertical components of the wave activity flux respectively; p is pressure, φ and λ are latitude and longitude respectively, u and v are zonal and meridional winds, Ω is the Earth's rotation rate, a is the Earth's radius, Φ is geopotential, T is temperature and S is the static stability parameter. The prime denotes perturbations from the zonal mean values.

140 The Madden-Julian oscillation (MJO) phase is determined using the seasonally independent Real-time Multivariate MJO index (RMM) [downloaded from Bureau of Meteorology \(http://www.bom.gov.au/climate/mjo/\)](http://www.bom.gov.au/climate/mjo/) for verification and from the [Subseasonal-to-Seasonal Prediction Project \(http://s2sprediction.net/\)](http://s2sprediction.net/) for the forecasts. It is based on time series of the two leading principal components derived from empirical orthogonal functions (EOFs) of the combined
145 fields of near-equatorially averaged 850 hPa zonal wind, 200 hPa zonal wind, and satellite-observed outgoing longwave radiation (OLR) data (Wheeler and Hendon, 2004). The RMM index is divided into eight phases that broadly correspond to the regions of enhanced convection.

3 Results

3.1 Stratospheric forecasts

150 We start by analysing the predictability of SSW2018 in the ECMWF ensemble forecast. Figure 1 shows the temporal evolution of the observed and forecasted zonal mean zonal wind at 10 hPa and 60° N (U10) for individual ensemble members during February 2018. In the forecast initialized on 1 February, there is a weak SSW signal: 14 ensemble members (~27 %, orange dashed lines) predicted wind reversal within 1 day from the observed onset date. The forecasted SSW probability, defined as
155 a fraction of ensemble members predicting an SSW at each day (Karpechko, 2018; Taguchi, 2016; Tripathi et al., 2016), was 0.06 on the observed onset date of 12 February and increased to 0.31 by 14 February when the minimum values of U10 were achieved by most ensemble members. The spread of predicted wind speed among the members increases markedly after 9 February when the observed polar night jet underwent the strongest deceleration. The fluctuations of the easterlies observed in the

160 reanalysis after the reversal are not captured by any ensemble members. Karpechko et al. (2018) showed that most ensemble members underestimated the eddy heat flux at 100 hPa which is used to characterize the upward planetary wave propagation from the troposphere to the stratosphere since it is proportional to the vertical group velocity of a planetary wave and to the vertical component of the Eliassen-Palm flux (Newman et al., 2001).

165 The evolution of zonal mean zonal winds at 10 hPa for February 2018 is shown in Fig. 2. Early in the month, the axis of the polar night jet is located at around 70° N and shifting gradually poleward (Fig. 2a). On 11 February, the jet quickly decelerates around 80° N and the zonal wind reversal occurs in high latitudes and extends from the North Pole to about 50° N. Easterly wind peaks of – 30 m/s are found on 12–16 February and around 21 February after diminishing to zero on 17 February at 60° N.
170 The northward shift of the polar night jet occurs prior to the zonal wind reversal – a feature highlighted in some previous SSW studies and pointed out as a precondition for the effective wave forcing because in this case the relatively small mass and moment of inertia of the vortex allow upward propagating waves to distort it (Limpasuvan et al., 2004; McIntyre, 1982; Harada et al., 2010; Nishii et al., 2009). [The position of the vortex close to the pole and little vertical tilt are typical for the split SSWs as was pointed out by](#) Albers and Birner (2014). Overall, easterly winds dominate the polar stratosphere north of 50° N from mid-February to March.

The composite of the ENS₊ members (Fig. 2b) captures well the northward shift of the polar jet axis in the beginning of the February and the wind reversal on 12 February. The composite mean underestimates the magnitude and duration of easterlies, recovering to westerly flow after 18
180 February. This could possibly reduce the forecasted impacts of SSW2018 on surface. ~~Several~~ [Two](#) ensemble members, however, maintained easterlies until the end of February matching the magnitude of the observed easterlies [although neither of them captured the timing of the observed zonal mean zonal wind oscillation during the negative phase](#) (Fig. 1). The ENS₋ composite (Fig. 2c) maintains westerlies throughout February.

185 Figure 3 shows that in the beginning of February, the centre of the polar vortex is already displaced from the pole towards Greenland and Norwegian sea and a high over the Alaska begins to develop. During 4–6 February the two troughs over Northern America and Central Siberia and the anticyclone over Alaska start to form [\(not shown\)](#). By 7–9 February another high over the North Atlantic begins to develop (wavenumber 2 planetary wave pattern, Fig. 3a). During 10–12 February the two highs
190 merge over the pole leading to a vortex split. The low over Canada intensifies while the other part of the split vortex weakens over Siberia, leading to the circulation reversal at 60° N (Fig. 3d). To reveal forecast errors we compare the ENS₊ and ENS₋ members composites to the reanalysis (Fig. 3 b,c,e,f). Analysis shows that during the first ~7 days after the initialization the forecast errors in the

stratosphere are modest, consistent with the analysis of Karpechko (2018), but they start to grow after
195 7 February mainly near the position of one of the daughter vortices over Northern America in both
| [ENS+](#) and [ENS-](#) clusters (Fig. 3 b, c). By 10–12 February, the [ENS-](#) cluster notably underestimates
| the magnitude of the merged high that had replaced the polar vortex over the pole, and it shows bigger
| errors in the position of the cyclone over Canada (Fig. 3f) compared to the [ENS+](#) cluster (Fig. 3e).
However, the overall structure of the errors appears remarkably similar in the two groups which might
200 suggest the presence of a systematic model bias.

Long planetary waves are known to interact with the mean flow before SSWs (e.g. Limpasuvan et
al., 2004). Time evolution of the planetary waves amplitudes in the beginning of the February 2018
is shown in Fig. 4. The highest wave activity in the NH stratosphere is concentrated within the
latitudinal range of 40° N – 75° N (e.g. Peters et al., 2010), therefore this belt of latitudes was chosen
205 for averaging. Planetary wave with wavenumber 1 (PW1) dominates in the beginning of February in
the middle stratosphere, but its amplitude decreases rapidly and reaches its minimum on 10 February.
On the other hand, the amplitude of PW2 starts to grow rapidly on 4 February reaching values of 90
dam on 10 February just before the SSW2018 onset (Fig. 4a). Such inverse correlation of these two
planetary waves is often observed before major split type SSWs as the propagation characteristics of
210 the waves differ depending on the zonal wavenumber and wave period (Charney and Drazin, 1961).
| [Moreover, the amplitude vacillation between PW1 and PW2 may be caused by wave-wave](#)
| [interactions](#) (Smith, 1983). A strong PW2 increase often results in a vortex splitting (McIntyre, 1982),
as it happened in February 2018. Figures 4b and c depict the time evolution on the first three waves
for the each of the 10 chosen [ENS+](#) and [ENS-](#) members. First, the evolution across individual
215 ensemble members in both categories is remarkably similar, though the spread in the [ENS-](#) cluster is
bigger. The overall evolution pattern in the [ENS+](#) cluster resembles well the ERA-I verification (Fig.
4b). The [ENS-](#) members fail to capture the amplitude growth of the PW1 after 10 February and, in
addition to that, they underestimate the PW2 amplitude (Fig. 4c). PW3 remains weak in both
observations and forecast ensembles.

220 On 7 February the polar vortex had already been weakened and distorted (Fig. 3a) and the polar
night jet started to decelerate. Horizontal distribution of the ensemble spread in the lower stratosphere,
| [represented by the standard deviation of the ensemble members](#) is shown in Fig. 5. The largest
| ensemble spread is mainly confined to the subpolar North Atlantic (Fig. 5a) where the forecast errors
| on that date are the largest (Fig. 3c). Throughout the period of vortex deceleration the area of the large
225 forecast spread at 50 hPa height gradually expands horizontally and, by 12 February, it covers most
of the polar stratosphere north of 70° N (Fig. 5b,c).

To better understand sources of ensemble spread in the stratosphere we look at the zonal cross-sections (Fig. 6). As seen in Fig. 6a, there are three areas of large ensemble-forecast spread on 7 February, when the polar vortex started to decelerate and be distorted: over the Ural Mountains, Alaska and North Atlantic regions. The areas with the large spread extend from the troposphere into the lower stratosphere. Blocking anticyclones in these regions were pointed out to be associated with SSW tropospheric forcing (Martius et al., 2009; Woollings et al., 2010; Rao et al. (2018); Karpechko et al., 2018), as they may act as the source of the Rossby-wave packets that propagate into the stratosphere and lead to a SSW onset. The upward group velocity propagation of the waves is indicated by the westward tilt of the geopotential anomaly lines with height (Fig. 6). The spread can be explained by the inconsistencies in the location, amplitudes and group velocities predicted by different ensemble members (Nishii and Nakamura, 2010). In fact, most of the ensemble members started to underestimate the heat flux entering the stratosphere (Fig. 1 in Karpechko et al., 2018) after 7 February.

To further analyse contribution of these three regions to the SSW2018 forcing we examine the timeseries of the vertical component of wave activity flux averaged zonally and over the three continuous longitudinal ranges. The main wave event is identifiable in lower and middle stratosphere prior to the circulation reversal (Fig. 7a), preceded by the upward flux maxima in the lower and mid-troposphere on 4 February with the time lag of ~7 days needed for the planetary wave to propagate vertically from the troposphere to the stratosphere. The division into three longitudinal ranges allows us to investigate the wave activity flux propagation between the troposphere and the lower and middle stratosphere over the limited longitudinal ranges (Harada et al., 2010; Coy and Pawson, 2015). The North Atlantic ~~third~~-sector (Fig. 7j) shows the biggest maxima of vertical wave activity flux in the troposphere in the beginning of February and also in the lower and middle stratosphere just before the SSW onset compared to the other two thirds of the globe. ~~The similar~~Strong upward-propagation ~~pattern~~ can also be seen in the stratosphere in the Europe/Siberia ~~third~~-sector, which likely contributed to initial weakening of the vortex (Fig. 7d). The North Pacific ~~third~~-sector (Fig. 7g) shows an increased upward flux before the event which is restricted to the lower stratosphere. Additional analysis showed that wavenumber 2 was the largest contributor to the upward wave activity during the week preceding SSW while wavenumber 1 was the largest contributor until 3–5 February (not shown), in agreement with wave amplitude evolution shown in Figure 4. Note that, enhanced tropospheric forcing, in addition to directly affecting the mean stratospheric circulation, may also alter the geometry of the vortex and precondition it to splitting by triggering the internal resonance (Albers and Birner, 2014).

Comparison of the similar diagnostics of vertical WAF performed for the ENS₊ and ENS₋ composites (Fig. 7, 2 and 3 column respectively) shows that the ENS₊ cluster captures the wave

propagation patterns zonally averaged (Fig. 7b) and in all three longitudinal ranges (Fig. 7 e, h, k) although it somewhat underestimates the magnitudes of fluxes. The ENS_– forecasts composite does not predict a significant vertical wave propagation from the troposphere into the stratosphere in either of the longitudinal ranges.

265 While the ENS_– forecasts failed to reproduce the increases in wave activity flux in all three regions, it is not clear where the errors were crucial for the failed SSW forecast. The correlation analysis of the zonal mean WAF at each level averaged over 4–11 February with forecast U10 on 12 February across individual ensemble members shows the negative correlation at all levels, starting from the lower troposphere, at 0.05 significance level (Fig. 8a). The correlation coefficient increases
270 with height reaching $r = -0.95$ at 50 hPa. When split into the three regions, the wave activity contributions from the Siberia and North Atlantic sectors are significant in the lower and middle stratosphere, with strongest correlations found in the Siberian sector (Fig. 8b). This suggests that upward wave activity propagation in these regions was critical for the SSW2018 forcing. On the other hand, the correlation analysis shows that there is no significant relation between WAF in the North
275 Pacific sector and U10.

3.2 Tropospheric waves

We next look at the tropospheric precursors of SSW2018. The three areas with the largest forecast spread (Fig. 6) are associated with blocking ridges seen in the 250 hPa geopotential height (Fig. 9a). Several wave packets manifested as meandering westerlies can be distinguished in the consecutive
280 geopotential height fields over the period of 3–9 February (coloured lines). Most pronounced one is associated with the anticyclonic wave breaking episode over the North Atlantic (red line) also demonstrated by Lee et al. (2019). Here, a well-developed ridge can be seen on 3 February. During 4–6 February this ridge breaks anticyclonically and forms a cut-off anticyclone over Scandinavia on 6 February which continued propagating downstream until blocked ~~by the developing anticyclonic~~
285 ~~ridge~~ over the Ural region around ~~6~~7–7 February after which time it remained quasi-stationary until 9 February (red line). The second ridge (blue line) can be distinguished propagating across North Atlantic during 5–8 February until decayed over Spain on 9 February. The developing of this wave might be traced back in squared meridional wind to western North America on 4 February ~~in squared meridional wind~~ (dashed blue line in Fig. 9b). ~~–and propagating downstream during 5–8~~
290 ~~February~~. Finally, a trough can be seen propagating across North America during 7–9 February (yellow line). Its development can also be traced in squared meridional wind back to western North

[America on 6 February](#). At the same time a stationary upper troposphere ridge is seen over Alaska over the whole period ([green line](#)).

295 The propagation of the synoptic features can be also diagnosed using the squared meridional wind fields (Nishii and Nakamura, 2010). Figure 9b shows that, between 3 and 7 February, the maximum of the squared 250 hPa meridional wind propagated across the North Atlantic and Northern Eurasia with an average group speed of $\sim 27^\circ$ in longitude per day before being blocked over the Urals with little downstream propagation thereafter. Such propagation speed is consistent with group velocity of baroclinic waves (Chang, 1993; Nishii and Nakamura, 2010) suggesting that formation of the
300 blocking anticyclone was the result of a downstream development. Figure 9b also shows that the stationary Alaskan ridge served as a source of two more individual wave packets that propagated towards the Atlantic starting on 3 and 6 February respectively.

The ENS₊ composite of the squared meridional wind at 250 hPa (Fig. 10a) is in agreement with the reanalysis (Fig. 9b), capturing all three wave packets discussed above, whereas in the ENS₋
305 cluster the wave train over the Ural region disappears starting from 6 February. Thus, the wave packet associated with the Ural blocking fades away in the ENS₋ members. Although the propagation of other wave packets is captured by the ENS₋ cluster, there are differences with respect to the ENS₊ cluster in the location and magnitude of the packets. In particular the magnitude of the Atlantic ridge on 6–9 February is strongly underestimated. The differences between the ENS₊ and ENS₋ clusters
310 can also be investigated by looking at the forecast spread in the meridional wind at 250 hPa that represent inconsistency among the ensemble members (Fig. 10c). Downstream propagation of the forecast spread is well distinguishable in the Fig. 10c and it is strongly associated with the propagation of the aforementioned wave packets. Interestingly, there is large spread also in the eastern Pacific associated with the quasi-stationary Alaskan ridge.

315 To see the behaviour of the wave packets in more detail we studied the horizontal propagation of WAF (~~Plumb, 1985~~). The observed wave activity in the mid-troposphere and the difference between the ENS₊ and ENS₋ clusters are shown in Fig. 11 for 5–7 February. We focus on this time period because this is when large differences between these two ensembles have emerged and we use 3-day averaging following previous practices of using this diagnostic developed for quasi-stationary waves
320 (e.g. Harada et al., 2010; Peters et al., 2010). The 500 hPa pressure level is chosen to highlight the mid-tropospheric processes. The same diagnostics in the upper troposphere (300 hPa) yield similar results (not shown). Figure 11a shows eastward propagation of wave activity along the jet stream in the reanalysis, with large values seen in all three regions of anomalous highs identified in the previous sections. [The wave activity propagation in the ENS₊ members group is reasonably similar to the reanalysis \(Fig. 11b\). However,](#) the eastward ~~wave activity propagation-WAF~~ is stronger in
325

the ENS₊ members compared to ENS₋ through most of the NH extratropics with the greatest differences following the meandering extratropical jet stream (Fig. 11c**b**). Remarkable difference in the horizontal propagation of wave packets is seen over all three centres of forecast uncertainty discussed above – Alaskan, North Atlantic and Ural suggesting underestimation of eastward wave activity propagation in the ENS₋ cluster. To inspect closely the difference in wave propagation between the ENS₊ and ENS₋ clusters we look at the magnitude of the horizontal wave flux within the areas representative for these regions marked in Fig. 11c**b** as two boxes (over the Ural region (Box 1) and the North Atlantic (Box 2)). Over the North Pacific, since the anomalous flux changes its direction within the area, we choose to analyse the flux through the two surface lines (Fig. 12). The wave activity propagation over the Box 1 in the ENS₊ cluster captures well the sharp amplification seen in the ERA-I verification between 5–9 February and somewhat overestimates its magnitude. This amplification corresponds to the period of the development of the Ural blocking high (Fig. 12a). The ENS₋ cluster fails to capture this intensification of the wave activity. The wave activity fluxes through the surfaces defined by the Lines 1 and 2 (Fig. 12b,c) are comparable between the ENS₊ and ENS₋ clusters and reproduce the fluctuations seen in ERA-I, ~~but in general they underestimate the observed values~~. Note that this result is not sensitive to the exact location of the lines. The analysis of the net flux in the North Atlantic region (Box 2) ~~does not show significant differences between the ensemble members and ERA-I~~: shows the ~~two~~three individual peaks between ~~34~~ and ~~910~~ February, corresponding to the joint effect of the three individual wave packets revealed in Fig. 9–10, which are somewhat underestimated in both ensemble members groups~~are well captured in the forecast~~ (Fig. 12d). Thus, results in Fig. 12 suggest that the key difference between the ENS₊ and ENS₋ forecasts in terms of horizontal wave activity propagation is in the Ural region.

To demonstrate that the differences in horizontal WAF in the mid-troposphere between the ENS₊ and ENS₋ clusters are relevant for SSW forecasting we perform the correlation analysis of zonal mean zonal wind in the mid-stratosphere and the zonal component of WAF at 500 hPa across all ensemble members. Over the Northern Siberia, the correlation field (Fig. 13) resembles the location of the biggest differences in WAF between the ENS₊ and ENS₋ clusters (Fig. 11) with statistically significant negative correlation coefficients exceeding -0.5 . Thus, the negative correlation in the Ural region indicates that the stronger flux in the region is associated with weaker stratospheric winds and suggests that errors in the wave activity in the location of the Ural high turn out to be crucial for forecasting SSW2018, consistent with the results by Karpechko et al. (2018) and Lee et al. (2019).

3.3 Teleconnection with MJO

~~In the 10-day period~~ before the SSW2018 central date (~~27 January–7 February~~) an active MJO in phases 6 and 7 with large amplitude prevailed in tropical Indian ocean and South China Sea (Barrett, 2019). It has been shown that MJO phase 6/7 events associated with OLR anomalies in Eastern Pacific can lead to the weakening of the polar vortex through enhancement of upward propagating wave fluxes towards Alaska and are often followed by SSWs (Schwartz and Garfinkel, 2017). In this section we assess the evidence that the MJO played a role in the onset of SSW2018. We chose for the analysis the ensemble forecast initialized on the 1 February and, as the amplification of the MJO phase 6 occurred prior to that date, it is expected that the wave activity source associated with MJO has been included into forecast initial conditions, potentially leading to the more precise forecast of SSW2018. We find no evident link between the skill of MJO forecast and SSW2018: the ENS₊ members do not predict MJO more correctly than the ENS₋ members (see Fig. A2 in Appendix A). Based on that we focus on analysis of MJO teleconnections, testing the hypothesis that correct forecasting of MJO teleconnections was important factor in simulating SSW2018.

To verify that, first, we constructed the composite field of geopotential height anomalies picked only for days with MJO phase 6 with the lag of 5–9 days in both ECMWF historical forecasts and ERA-I. It is very difficult to clearly establish the causality between tropical oscillations and polar anomalies, because of the complex interactions between the propagating waves and the mean flow. Therefore, one of the ways to approach causality is to use time lag. The lag of 5–9 days after MJO phase 6, which took place on 27–31 January, roughly corresponds to the period in the early February when tropospheric waves forced SSW2018 based on the analysis in the previous sections. In particular, the ridge over the North Atlantic was developing during this period. This suggests that the MJO phase 6 fingerprint should be taken with the lag of 5–9 days.

We start by testing how well can the model reproduce MJO phase 6 teleconnection in the extratropics. In Fig. 14a contours represent the composite fields showing the ~~observed climatological ERA-I~~ fingerprint of the MJO phase 6 ~~are presented with contours~~. Contours in Figures 14 b and c show similar fingerprint but constructed with the model hindcasts over ~~20 years~~ the 20-years period. These two fields both have prominent lows in the North Pacific and over Canada and highs over the Ural, western North America and the North Atlantic. Although the fingerprint fields show some dissimilarity in the positions and strength of the features, their overall structure is well captured by the model. This result is in line with Vitart (2014, 2017) who showed that the model produces realistic patterns of MJO teleconnections.

Figure 14a also shows the observed geopotential anomalies field averaged for 5–7 February (shading), i.e. 5–7 days after the end of the MJO phase 6. Although ~~the spatial correlation between the two fields is small ($r=0.03$), likely because~~ the key features in 2018 are somewhat displaced with

395

400

405

410

415

420

respect to the climatological composite, the overall structure of the field prior to SSW2018 strongly resembles the climatological MJO response, capturing the anomalous highs over the Siberia, high-latitude Pacific and North Atlantic, as well as the low over the Canada. [The spatial correlation between the two fields \(climatological lagged composite for phase 6 and anomalies observed on 5–7 February 2018\) in the extratropics \(40° N–90° N\) is \$r=0.32\$ and significant at 0.01 level.](#) On the other hand, the low in the North Pacific region is not pronounced and the high over western America is displaced towards northwest. Although the evidence is not conclusive, ~~analysis of Fig. 14a~~ [the similarity between the pattern observed in early February 2018 and the climatological MJO phase 6 signal](#) support the idea that MJO teleconnections may have played a significant role in dynamical evolution of the extratropical atmosphere [during early February 2018, and therefore could contribute to forcing of](#) ~~preceding~~ SSW2018, consistent with existing literature (Schwartz and Garfinkel, 2017).

The composite field made for 5–7 February 2018 using the ENS₊ members captures the observed structure of geopotential height field well with PW2 pattern prevailing in the northern latitudes, and also strongly resembling the MJO fingerprint composite (Fig. 14b). On the contrary, the response in the ENS₋ cluster ~~does not resemble either the observed field or the MJO composite and~~ shows a PW1 pattern with two highs in Alaska and Ural region merged together (Fig. 14c), which is consistent with the ENS₋ forecasts not capturing the amplification of PW2 in the stratosphere (Fig. 4c). In summary, our composite analysis provides supportive, although not decisive, evidence that teleconnections associated with MJO phase 6 played a role in triggering SSW 2018 both in observations and in the forecasts.

4 Discussion and Conclusions

Using the ECMWF ensemble forecast we examined the predictability of the major SSW in the middle of February 2018. We focused on the identification of the involved dynamical processes and studied the role of the tropospheric forcing leading to the polar vortex split.

First, we have selected two groups of ensemble members based on the zonal mean zonal wind at 10 hPa and 60° N metric to discern spatial and temporal distribution of forecast errors and its possible sources by comparing the ensemble composites to the reanalysis fields. SSW2018 was preceded by the amplification of PW2 and record-breaking eddy heat flux in the lower stratosphere. This amplification was reasonably well captured by forecast ensemble members predicting SSW2018 but not those that did not predict it (Figure 4). The forecast error in geopotential height in the mid-stratosphere is small until 7 February and starts to grow mainly near the edge of the polar vortex following its displacement towards North America (Figure 3), marked also by the largest ensemble

spread (Figure 5). The growth of the forecast spread was linked to the positions of tropospheric
425 blocking ridges (Figure 6) suggesting that their accurate prediction was important for forecasting the
SSW2018 event. The amplification of the stratospheric PW2 was related to a PW2 pattern in the mid-
troposphere and was apparently brought about by accumulative effects of localized propagation of
wave packets. The period preceding SSW2018 was characterized by the enhanced wave activity in
the troposphere. In the Pacific region wave activity fluxes maintained quasi-stationary ridge over
430 Alaska (Figure 7). Over North Atlantic, eastward propagation of individual wave packets could be
identified and tracked back to the Alaskan ridge which served as their source. We show that the
propagation of the forecast uncertainties is associated with the downstream propagation of these
synoptic patterns in the troposphere, and the subsequent upward propagation of the wave packets to
the stratosphere. Comparison of the ENS+ and ENS- forecast composites reveals that the ENS+
435 forecasts correctly captured the whole chain of the observed events, from downstream propagation
of individual wave packets, to the upward propagation of wave activity, amplification of stratospheric
PW2 and breaking down of the stratospheric polar vortex. On the other hand, our analysis suggests
that ENS- members underestimated both horizontal and vertical WAF propagation. In particular, it
is found that the development of the upper troposphere blocking anticyclone over the Ural region
440 around 6–7 February following the energy injection from wave breaking over North Atlantic during
4–6 February was largely missing in the ENS- cluster. This wave breaking event was also highlighted
by Lee et al., (2019) as being important for amplifying a high-pressure system over the Urals and
triggering SSW2018. [We have also shown that the wave packet crucial for the formation of the Ural
blocking is not captured by the ensemble members that failed to forecast SSW2018.](#) ~~Here we also
445 have showed that the crucial for the Ural blocking wave packet does not appear in the ensemble
members that failed to capture SSW2018.~~ According to our statistical analysis, forecasted
stratospheric winds are mostly correlated with horizontal zonal wave activity flux over the Ural
region, with stronger WAF in that region being associated with weaker stratospheric winds (Figure
13). Furthermore, correlation analysis also reveals that weaker stratospheric winds in the forecast
450 were mostly associated with the vertical propagation of the wave activity flux over the Siberian sector
with a contribution from the North Atlantic sector (Figure 8). While we also find enhanced vertical
wave activity propagation from the Alaskan sector, correlation analysis of the forecast members
suggests that WAF over this region did not contribute to the SSW2018 forcing, which is somewhat
inconsistent with results by Rao et al., (2018), who concluded that SSW2018 is caused by the Alaskan
455 blocking.

SSW2018 was preceded by the highest ever observed MJO phase 6 which could create favourable
conditions for strengthened Rossby wave teleconnections between the tropics and the extratropics.

460 We have shown that the anticyclonic centres over the North Atlantic, Ural and Alaska regions formed before SSW2018 correspond to the MJO phase 6 response pattern taken with the lag of 5–9 days ([Figure 14](#)). These centres were captured well by the ENS₊ members while the ENS₋ cluster failed to reproduce the PW2 structure in the northern latitudes. The composite analysis provides ~~an~~ evidence, ~~although not decisive~~ [albeit indecisive](#), that teleconnections associated with MJO phase 6 played a role in triggering SSW2018.

465 We conclude by pointing out the importance of the accurate prediction of the strength and position of synoptic scale mid- and upper tropospheric features and understanding the origin of planetary wave anomalies for improving the prediction of SSW events. Though the predictability of the 1–2 weeks for SSW2018 falls within the usual range of predictability for the split events (Karpechko, 2018; Domeisen et al., 2019a), the exceptional conditions before the event could have potentially enhanced the predictability. It is important to understand what part of the forecast error was associated with 470 internal variability and what part was due to systematic bias, which is planned to be addressed in a follow up study.

Data availability. All data is available from the European Centre for Medium Range Weather Forecasting (ECMWF). See <https://apps.ecmwf.int/datasets/> for more details. Madden–Julian oscillation (MJO) phase is available from The Bureau of Meteorology: <http://www.bom.gov.au/climate/mjo/>. [MJO phase predicted by the ECMWF extended-range prediction system is available from the Subseasonal-to-Seasonal Prediction Project: http://s2sprediction.net/](#).

480 *Code availability.* Code is available from Irina Statnaia upon request.

Author contributions. IS performed data analysis and wrote the first draft of the manuscript. AK formed the idea for the study, contributed to the interpretation of the results, and improved the final manuscript. HJ provided guidance on interpreting the results. All authors commented on the 485 manuscript.

Competing interests. The authors declare that they have no conflict of interest.

Acknowledgements. [The authors are grateful to the three anonymous referees whose comments led to the improvement of this paper.](#) IS is funded by the Magnus Ehrnrooth Foundation and Finnish Meteorological Institute (FMI). AK is funded by the Academy of Finland (grants 286298, 294120, 490

and 319397). This work is based on (subseasonal-to-seasonal) S2S data. S2S is a joint initiative of the World Weather Research Programme (WWRP) and the World Climate Research Programme (WCRP).

495

References

- Albers, J. R. and Birner, T.: Vortex Preconditioning due to Planetary and Gravity Waves prior to Sudden Stratospheric Warmings, *J. Atmos. Sci.*, 71(11), 4028–4054, doi:10.1175/jas-d-14-0026.1, 2014.
- 500 Ayarzagüena, B., Barriopedro, D., Garrido-Perez, J. M., Abalos, M., de la Cámara, A., García-Herrera, R., Calvo, N. and Ordóñez, C.: Stratospheric Connection to the Abrupt End of the 2016/2017 Iberian Drought, *Geophys. Res. Lett.*, 45(22), 12,639–12,646, doi:10.1029/2018GL079802, 2018.
- 505 Baldwin, M. P. and Dunkerton, T. J.: Propagation of the Arctic Oscillation from the stratosphere to the troposphere, *J. Geophys. Res. Atmos.*, 104(D24), 30937–30946, doi:10.1029/1999JD900445, 1999.
- Barrett, B. S.: Connections between the Madden–Julian Oscillation and surface temperatures in winter 2018 over eastern North America, *Atmos. Sci. Lett.*, 20(1), 1–8, doi:10.1002/asl.869, 2019.
- 510 Butler, A. H., Seidel, D. J., Hardiman, S. C., Butchart, N., Birner, T. and Match, A.: Defining sudden stratospheric warmings, *Bull. Am. Meteorol. Soc.*, 96(11), 1913–1928, doi:10.1175/BAMS-D-13-00173.1, 2015.
- Castanheira, J. M. and Barriopedro, D.: Dynamical connection between tropospheric blockings and stratospheric polar vortex, *Geophys. Res. Lett.*, 37(13), 1–5, doi:10.1029/2010GL043819, 2010.
- 515 Chang, E. K. M.: Downstream development of baroclinic waves as inferred from regression analysis, *J. Atmos. Sci.*, 50(13), 2038–2053, doi:10.1175/1520-0469(1993)050<2038:DDOBWA>2.0.CO;2, 1993.
- Charlton, A. J. and Polvani, L. M.: A New Look at Stratospheric Sudden Warmings . Part I: Climatology and, *Am. Meteorol. Soc.*, 20, 449–470, 2007.
- 520 Charney, J. G. and Drazin, P. G.: Propagation of planetary-scale disturbances from the lower into the upper atmosphere, *J. Geophys. Res.*, 66(1), 83–109, doi:10.1029/jz066i001p00083, 1961.
- Christiansen, B.: Downward propagation and statistical forecast of the near-surface weather, *J. Geophys. Res.*, 110, 1–10, doi:10.1029/2004JD005431, 2005.
- 525 Coy, L. and Pawson, S.: The major stratospheric sudden warming of January 2013: Analyses and forecasts in the GEOS-5 data assimilation system, *Mon. Weather Rev.*, 143(2), 491–510, doi:10.1175/MWR-D-14-00023.1, 2015.
- Dee, D. P., Uppala, S. M., Simmons, A. J., Berrisford, P., Poli, P., Kobayashi, S., Andrae, U., Balmaseda, M. A., Balsamo, G., Bauer, P., Bechtold, P., Beljaars, A. C. M., van de Berg, L.,

- 530 Bidlot, J., Bormann, N., Delsol, C., Dragani, R., Fuentes, M., Geer, A. J., Haimberger, L., Healy, S. B., Hersbach, H., Hólm, E. V., Isaksen, L., Kållberg, P., Köhler, M., Matricardi, M., McNally, A. P., Monge-Sanz, B. M., Morcrette, J. J., Park, B. K., Peubey, C., de Rosnay, P., Tavolato, C., Thépaut, J. N. and Vitart, F.: The ERA-Interim reanalysis: Configuration and performance of the data assimilation system, *Q. J. R. Meteorol. Soc.*, 137(656), 553–597, doi:10.1002/qj.828, 2011.
- 535 Domeisen, D. I. V., Butler, A. H., Charlton-Perez, A. J., Ayarzagüena, B., Baldwin, M. P., Dunn-Sigouin, E., Furtado, J. C., Garfinkel, C. I., Hitchcock, P., Karpechko, A. Y., Kim, H., Knight, J., Lang, A. L., Lim, E.-P., Marshall, A., Roff, G., Schwartz, C., Simpson, I. R., Son, S.-W. and Taguchi, M.: The role of the stratosphere in subseasonal to seasonal prediction Part I: Predictability of the stratosphere, *J. Geophys. Res. Atmos.*, n/a(n/a), doi:10.1029/2019JD030920, 540 2019a.
- Domeisen, D. I. V., Butler, A. H., Charlton-Perez, A. J., Ayarzagüena, B., Baldwin, M. P., Dunn-Sigouin, E., Furtado, J. C., Garfinkel, C. I., Hitchcock, P., Karpechko, A. Y., Kim, H., Knight, J., Lang, A. L., Lim, E., Marshall, A., Roff, G., Schwartz, C., Simpson, I. R., Son, S. and Taguchi, M.: The role of the stratosphere in subseasonal to seasonal prediction Part II: Predictability 545 arising from stratosphere - troposphere coupling, *J. Geophys. Res. Atmos.*, 125, 2019JD030923, doi:10.1029/2019JD030923, 2019b.
- Garfinkel, C. I., Feldstein, S. B., Waugh, D. W., Yoo, C. and Lee, S.: Observed connection between stratospheric sudden warmings and the Madden-Julian Oscillation, *Geophys. Res. Lett.*, 39(17), 1–5, doi:10.1029/2012GL053144, 2012.
- 550 Harada, Y., Goto, A., Hasegawa, H., Fujikawa, N., Naoe, H. and Hirooka, T.: A Major Stratospheric Sudden Warming Event in January 2009, *J. Atmos. Sci.*, 67(6), 2052–2069, doi:10.1175/2009jas3320.1, 2010.
- Holton, J. R. and Tan, H.-C.: The Influence of the Equatorial Quasi-Biennial Oscillation on the Global Circulation at 50 mb, *J. Atmos. Sci.*, 37(10), 2200–2208, doi:10.1175/1520- 555 0469(1980)037<2200:tioteq>2.0.co;2, 1980.
- Karpechko, A. Y.: Improvements in statistical forecasts of monthly and two-monthly surface air temperatures using a stratospheric predictor, *Q. J. R. Meteorol. Soc.*, 141(691), 2444–2456, doi:10.1002/qj.2535, 2015.
- Karpechko, A. Y.: Predictability of sudden stratospheric warmings in the ECMWF extended-range 560 forecast system, *Mon. Weather Rev.*, 146(4), 1063–1075, doi:10.1175/MWR-D-17-0317.1, 2018.
- Karpechko, A. Y., Charlton-Perez, A., Balmaseda, M., Tyrrell, N. and Vitart, F.: Predicting Sudden Stratospheric Warming 2018 and Its Climate Impacts With a Multimodel Ensemble, *Geophys.*

- Res. Lett., 45(24), 13,538-13,546, doi:10.1029/2018GL081091, 2018.
- 565 Kautz, L. A., Polichtchouk, I., Birner, T., Garny, H. and Pinto, J. G.: Enhanced extended-range predictability of the 2018 late-winter Eurasian cold spell due to the stratosphere, *Q. J. R. Meteorol. Soc.*, 146(August 2019), 1040–1055, doi:10.1002/qj.3724, 2019.
- Kuroda, Y. and Kodera, K.: Role of planetary waves in the stratosphere-troposphere coupled variability in the northern hemisphere winter, *Geophys. Res. Lett.*, 26(15), 2375–2378, 570 doi:10.1029/1999GL900507, 1999.
- De La Cámara, A., Birner, T. and Albers, J. R.: Are sudden stratospheric warmings preceded by anomalous tropospheric wave activity?, *J. Clim.*, 32(21), 7173–7189, doi:10.1175/JCLI-D-19-0269.1, 2019.
- Lee, S. H., Charlton-Perez, A. J., Furtado, J. C. and Woolnough, S. J.: Abrupt stratospheric vortex 575 weakening associated with North Atlantic anticyclonic wave breaking, *J. Geophys. Res. Atmos.*, 2019JD030940, doi:10.1029/2019JD030940, 2019.
- Limpasuvan, V., Thompson, D. W. J. and Hartmann, D. L.: The life cycle of the Northern Hemisphere sudden stratospheric warmings, *J. Clim.*, 17(13), 2584–2596, doi:10.1175/1520-0442(2004)017<2584:TLCOTN>2.0.CO;2, 2004.
- 580 Lu, H., Pancheva, D., Mukhtarov, P. and Cnossen, I.: QBO modulation of traveling planetary waves during northern winter, *J. Geophys. Res. Atmos.*, 117(9), 1–15, doi:10.1029/2011JD016901, 2012.
- Martius, O., Polvani, L. M. and Davies, H. C.: Blocking precursors to stratospheric sudden warming events, *Geophys. Res. Lett.*, 36(14), 1–5, doi:10.1029/2009GL038776, 2009.
- 585 Matsuno, T.: A Dynamical Model of the Stratospheric Sudden Warming, *J. Atmos. Sci.*, 28(8), 1479–1494, doi:10.1175/1520-0469(1971)028<1479:admots>2.0.co;2, 1971.
- McIntyre, M. E.: Well do we Understand the Dynamics of Stratospheric Warmings?, *J. Meteorol. Soc. Japan*, 60(1), 37–65, doi:https://doi.org/10.2151/jmsj1965.60.1_37, 1982.
- Nath, D., Chen, W., Zelin, C., Pogoreltsev, A. I. and Wei, K.: Dynamics of 2013 Sudden 590 Stratospheric Warming event and its impact on cold weather over Eurasia: Role of planetary wave reflection, *Sci. Rep.*, 6(October 2015), 1–12, doi:10.1038/srep24174, 2016.
- Newman, P. A., Nash, E. R. and Rosenfield, J. E.: What controls the temperature of the Arctic stratosphere during the spring?, *J. Geophys. Res.*, 106(D17), 19999–20010, 2001.
- Nishii, K. and Nakamura, H.: Lower-stratospheric Rossby wave trains in the southern hemisphere: 595 A case-study for late winter of 1997, *Q. J. R. Meteorol. Soc.*, 130, 325–345, doi:10.1256/qj.02.156, 2004.
- Nishii, K. and Nakamura, H.: Three-dimensional evolution of ensemble forecast spread during the

- onset of a stratospheric sudden warming event in January 2006, *Q. J. R. Meteorol. Soc.*, 136(649), 894–905, doi:10.1002/qj.607, 2010.
- 600 Nishii, K., Nakamura, H. and Takafumi, M.: Modulations in the planetary wave field induced by upward-propagating Rossby wave packets prior to stratospheric sudden warming events: A case-study, *Q. J. R. Meteorol. Soc.*, 135, 39–52, doi:10.1002/qj.359, 2009.
- Peters, D. H. W., Vargin, P., Gabriel, A., Tsvetkova, N. and Yushkov, V.: Tropospheric forcing of the boreal polar vortex splitting in January 2003, *Ann. Geophys.*, 28(11), 2133–2148, 605 doi:10.5194/angeo-28-2133-2010, 2010.
- Polvani, L. M. and Saravanan, R.: The three-dimensional structure of breaking Rossby waves in the polar wintertime stratosphere, *J. Atmos. Sci.*, 57(21), 3663–3685, doi:10.1175/1520-0469(2000)057<3663:TTDSOB>2.0.CO;2, 2000.
- Quiroz, R. S.: The association of stratospheric warmings with tropospheric blocking, *J. Geophys. Res.*, 91(D4), 5277, doi:10.1029/jd091id04p05277, 1986. 610
- Rao, J., Ren, R., Chen, H., Yu, Y. and Zhou, Y.: The Stratospheric Sudden Warming Event in February 2018 and its Prediction by a Climate System Model, *J. Geophys. Res. Atmos.*, 123(23), 13,332–13,345, doi:10.1029/2018JD028908, 2018.
- Scaife, A. A., Karpechko, A. Y., Baldwin, M. P., Brookshaw, A., Butler, A. H., Eade, R., Gordon, 615 M., Maclachlan, C., Martin, N., Dunstone, N. and Smith, D.: Seasonal winter forecasts and the stratosphere, *Atmos. Sci. Lett.*, 17(1), 51–56, doi:10.1002/asl.598, 2016.
- Schwartz, C. and Garfinkel, C. I.: Relative roles of the MJO and stratospheric variability in North Atlantic and European winter climate, *J. Geophys. Res.*, 122(8), 4184–4201, doi:10.1002/2016JD025829, 2017.
- 620 Sigmund, M., Scinocca, J. F., Kharin, V. V. and Shepherd, T. G.: Enhanced seasonal forecast skill following stratospheric sudden warmings, *Nat. Geosci.*, 6(2), 98–102, doi:10.1038/ngeo1698, 2013.
- Smith, A. K.: Observation of Wave-Wave Interactions in the Stratosphere, *J. Atmos. Sci.*, 40, 2484–2496, doi:https://doi.org/10.1175/1520-0469(1983)040<2484:OOWWII>2.0.CO;2, 1983.
- 625 Song, K. and Son, S. W.: Revisiting the ENSO – SSW Relationship, *Am. Meteorol. Soc.*, 1, 2133–2143, doi:10.1175/JCLI-D-17-0078.1, 2018.
- Taguchi, M.: Predictability of major stratospheric sudden warmings: Analysis results from JMA operational 1-month ensemble predictions from 2001/02 to 2012/13, *J. Atmos. Sci.*, 73(2), 789–806, doi:10.1175/JAS-D-15-0201.1, 2016.
- 630 Taguchi, M. and Hartmann, D. L.: Increased occurrence of stratospheric sudden warmings during El Niño as simulated by WACCM, *J. Clim.*, 19(3), 324–332, doi:10.1175/JCLI3655.1, 2006.

- Takaya, K. and Nakamura, H.: A Formulation of a Phase-Independent Wave-Activity Flux for Stationary and Migratory Quasigeostrophic Eddies on a Zonally Varying Basic Flow, *J. Atmos. Sci.*, 58(6), 608–627, doi:10.1175/1520-0469(2001)058<0608:afoapi>2.0.co;2, 2001.
- 635 Thompson, D. W. J., Baldwin, M. P. and Wallace, J. M.: Stratospheric connection to Northern Hemisphere wintertime weather: Implications for prediction, *J. Clim.*, 15(12), 1421–1428, doi:10.1175/1520-0442(2002)015<1421:SCTNHW>2.0.CO;2, 2002.
- Tripathi, O. P., Baldwin, M., Charlton-Perez, A., Charron, M., Cheung, J. C. H., Eckermann, S. D., Gerber, E., Jackson, D. R., Kuroda, Y., Lang, A., McLay, J., Mizuta, R., Reynolds, C., Roff, G., 640 Sigmond, M., Son, S.-W. and Stockdale, T.: Examining the Predictability of the Stratospheric Sudden Warming of January 2013 Using Multiple NWP Systems, *Mon. Weather Rev.*, 144(5), 1935–1960, doi:10.1175/mwr-d-15-0010.1, 2016.
- Vitart, F.: Evolution of ECMWF sub-seasonal forecast skill scores, *Q. J. R. Meteorol. Soc.*, 140(683), 1889–1899, doi:10.1002/qj.2256, 2014.
- 645 Vitart, F.: Madden—Julian Oscillation prediction and teleconnections in the S2S database, *Q. J. R. Meteorol. Soc.*, 143(706), 2210–2220, doi:10.1002/qj.3079, 2017.
- Vitart, F., Ardilouze, C., Bonet, A., Brookshaw, A., Chen, M., Codorean, C., Déqué, M., Ferranti, L., Fucile, E., Fuentes, M., Hendon, H., Hodgson, J., Kang, H. S., Kumar, A., Lin, H., Liu, G., Liu, X., Malguzzi, P., Mallas, I., Manoussakis, M., Mastrangelo, D., MacLachlan, C., McLean, 650 P., Minami, A., Mladek, R., Nakazawa, T., Najm, S., Nie, Y., Rixen, M., Robertson, A. W., Ruti, P., Sun, C., Takaya, Y., Tolstykh, M., Venuti, F., Waliser, D., Woolnough, S., Wu, T., Won, D. J., Xiao, H., Zaripov, R. and Zhang, L.: The subseasonal to seasonal (S2S) prediction project database, *Bull. Am. Meteorol. Soc.*, 98(1), 163–173, doi:10.1175/BAMS-D-16-0017.1, 2017.
- Wheeler, M. C. and Hendon, H. H.: An All-Season Real-Time Multivariate MJO Index : Development of an Index for Monitoring and Prediction, *Mon. Weather Rev.*, 132, 1917–1932, 655 2004.
- Woollings, T., Charlton-Perez, A., Ineson, S., Marshall, A. G. and Masato, G.: Associations between stratospheric variability and tropospheric blocking, *J. Geophys. Res. Atmos.*, 115(6), 1–17, doi:10.1029/2009JD012742, 2010.

660

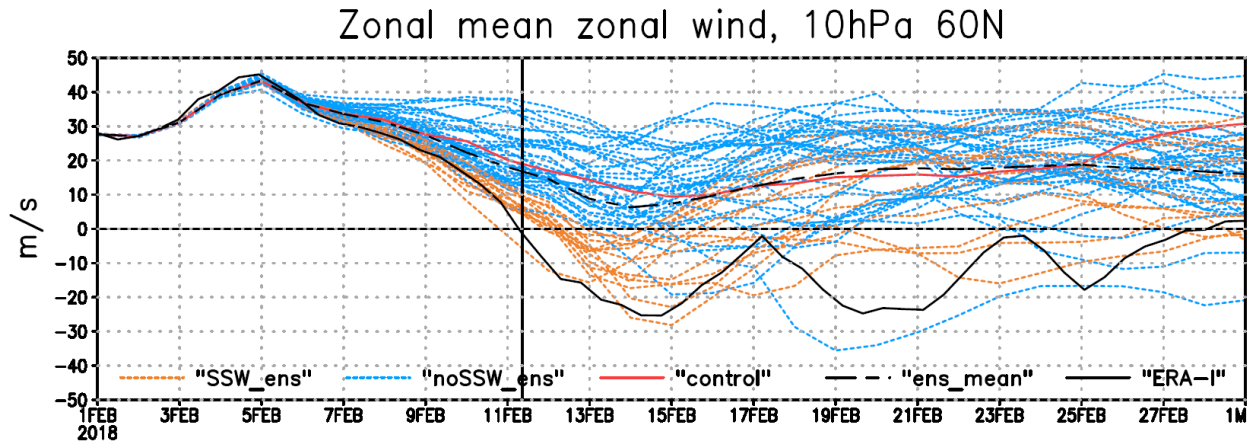
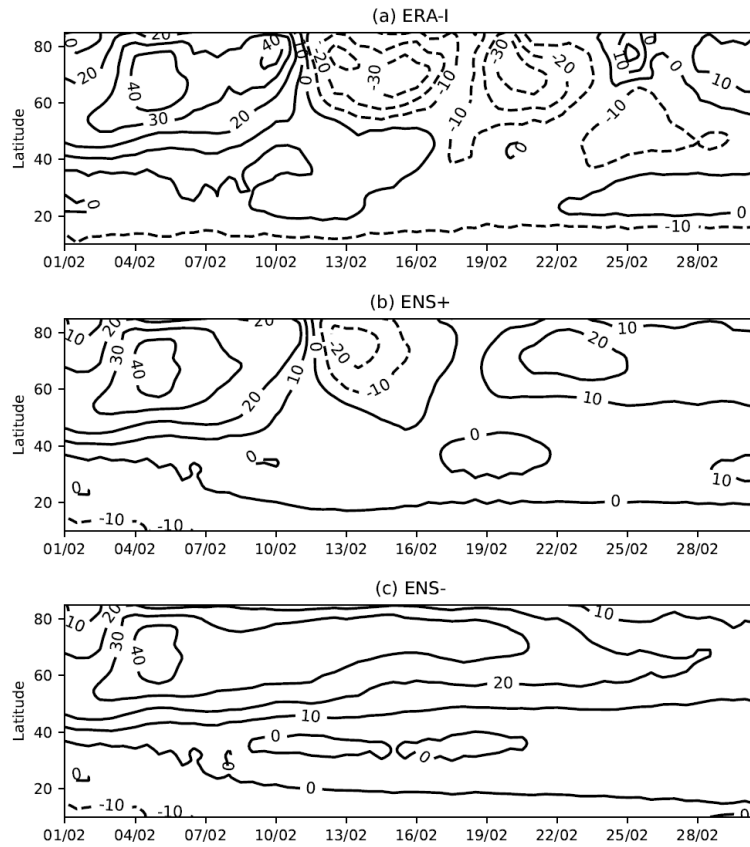
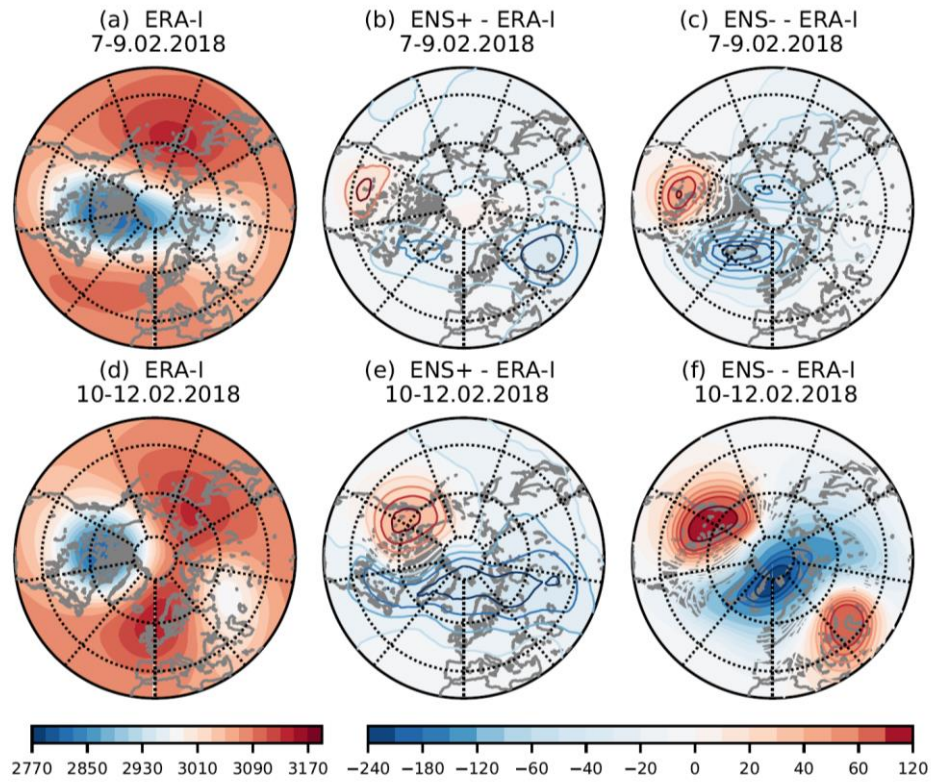


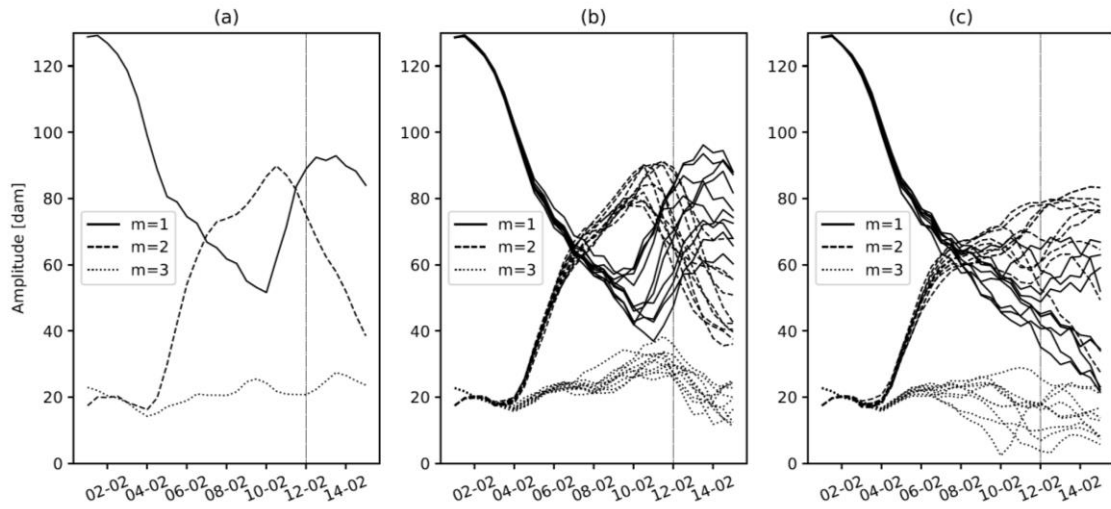
Figure 1. Zonal mean zonal wind at 10 hPa and 60° N (m s^{-1}). Ensemble forecast initialized on 1 February (orange lines denote ensemble members that predict wind reversal with max 1 day delay, red line – control forecast, black dashed line – ensemble mean) and the ERA-I reanalysis (black solid line). Vertical line denotes the SSW2018 central date.



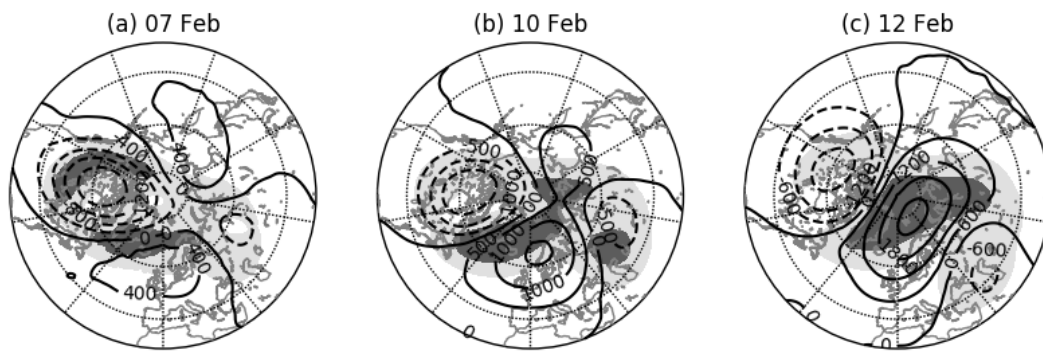
670 **Figure 2.** Latitude–time cross sections of zonal-mean zonal winds (m s^{-1}) at 10 hPa during February 2018. (a) ERA-I; (b) composite of ENS₊ members; (c) composite of ENS₋ members. Contour intervals are 10 m s^{-1} .



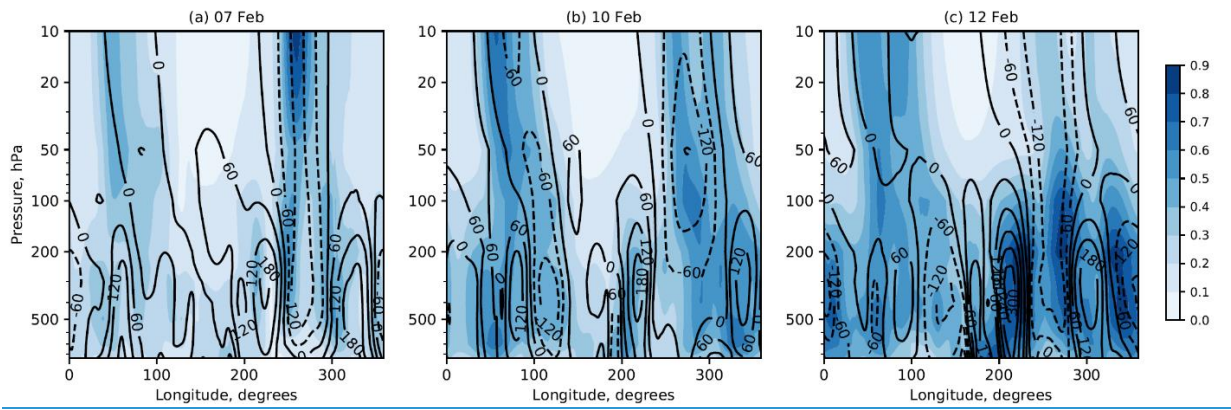
675 **Figure 3.** Geopotential height at 10 hPa (dam) for two successive 3-day means starting from 7 February (a, d). Difference in geopotential height at 10 hPa (dam) between ERA-I and ENS+ members (b, e) and ENS- members (c, f).



680 **Figure 4.** Time series of amplitudes of planetary waves with wavenumbers $m = 1, 2$ and 3 in geopotential height (dam) at 10 hPa averaged over the latitudinal belt $40^\circ \text{ N} - 75^\circ \text{ N}$ (a) ERA-I reanalysis, (b) ENS+ members, (c) ENS- members. Vertical line denotes the SSW2018 central date.



685 **Figure 5.** ERA-I 150 hPa geopotential height anomalies (contours, m) with respect to the 1980–2010 climatology and ensemble spread of geopotential height predicted for (a) 7, (b) 10 and (c) 12 February 2018 (shaded lightly and heavily for 0.3–0.6 values and values greater than 0.6, respectively). The spread has been normalized by the minimum and maximum values within the domain north of 20° N.



690 **Figure 6.** Zonal cross-sections for 50° N of the ensemble spread of geopotential height predicted for (a) 7, (b) 10 and (c) 12 February 2018. Superimposed contours represent observed geopotential anomalies (m) with respect to the 1980–2010 climatology. Solid lines represent anticyclonic (positive) anomalies and dashed lines cyclonic (negative) anomalies. ~~Spread and a~~Anomaly ~~are~~ is normalized by pressure.

695

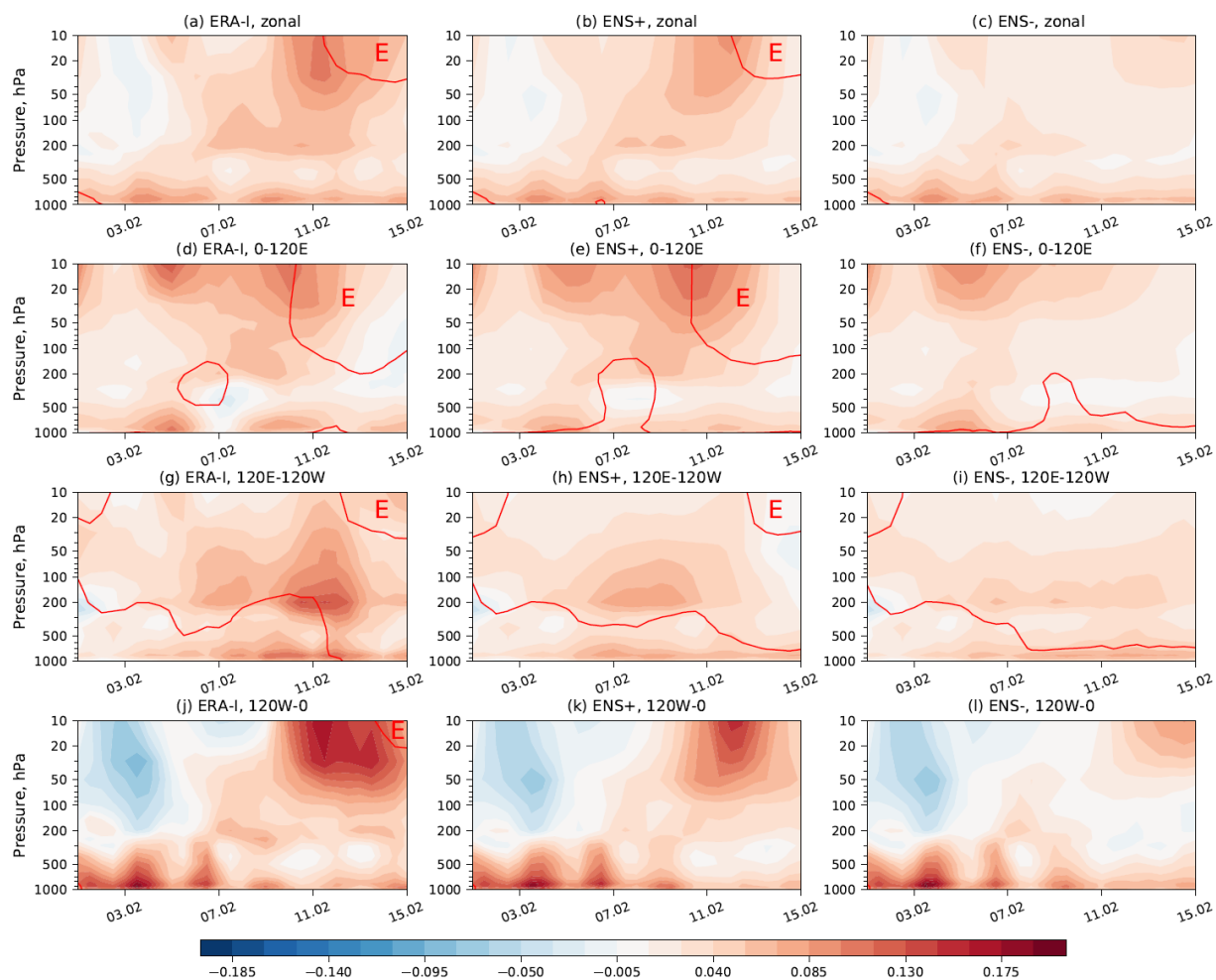


Figure 7. Time-altitude plot of the vertical component of WAF ($\text{m}^2 \text{s}^{-2}$, shaded, averaged over $45\text{--}90^\circ \text{N}$, vertically scaled by square root of 1000 hPa/p) and zero zonal wind contour (red) averaged over $55\text{--}65^\circ \text{N}$. (a–c) Zonally averaged, (d–f) averaged over $0^\circ\text{--}120^\circ \text{E}$, (g–i) averaged over $120^\circ \text{E}\text{--}120^\circ \text{W}$, (j–l) averaged over $120^\circ \text{W}\text{--}0^\circ$. The red letter ‘E’ denotes regions of easterly winds. (a, d, g, i) ERA-I; (b, e, h, k) ENS+ composite; (c, f, i, l) ENS– composite.

700

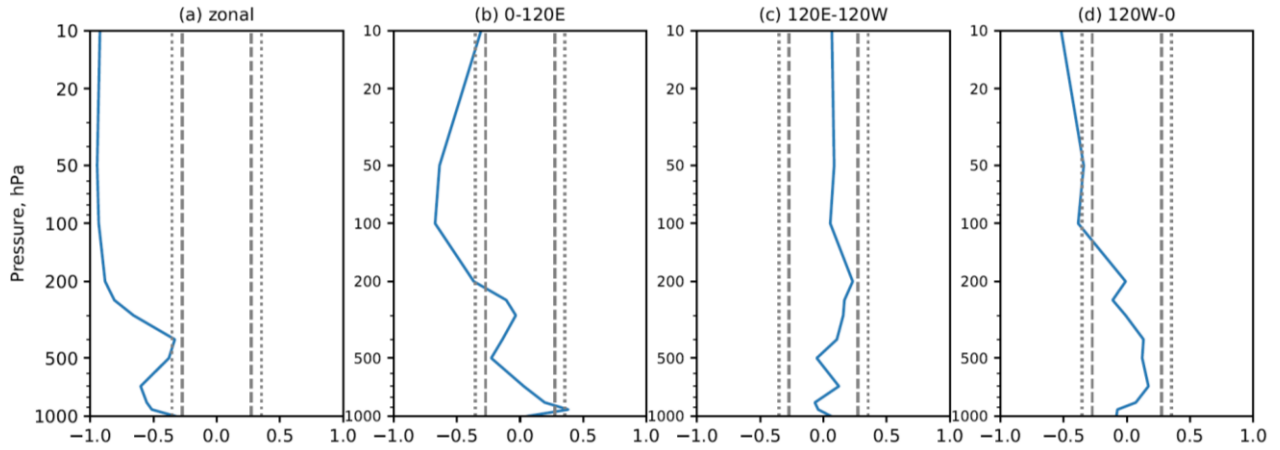
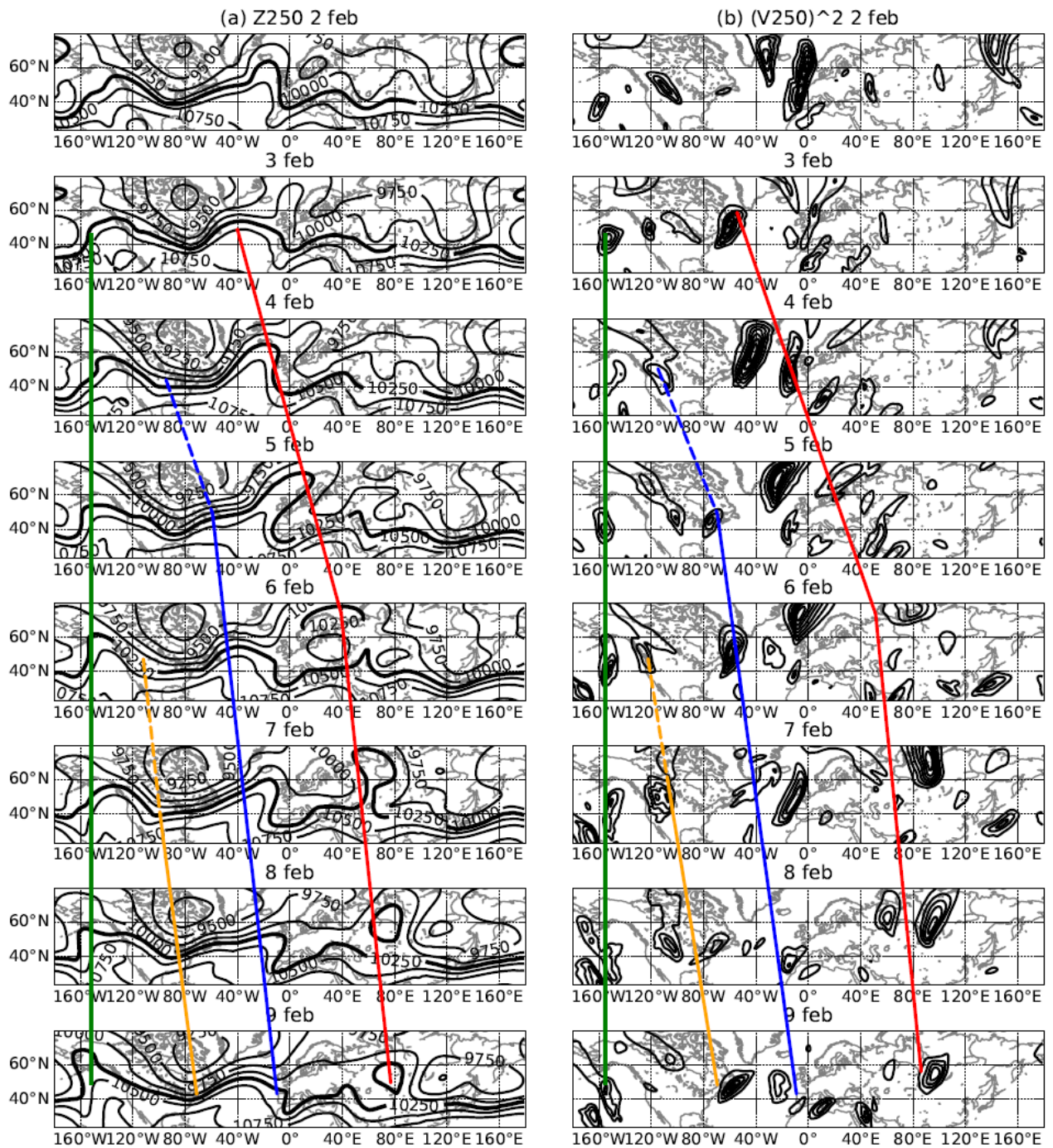


Figure 8. Vertical distribution of the correlation coefficient between the vertical component of the WAF forecasts averaged during 4–11 February and U10 forecasts valid on 12 February across individual forecast ensemble members. (a) Zonally averaged; (b) averaged over 0°–120° E; (c) averaged over 120° E–120° W; (d) averaged over 120° W–0°. Dashed vertical lines denote the 0.05 significance level, dotted vertical lines denote the 0.01 significance level.



710

Figure 9. Time sequence of (a) ERA-I 250 hPa geopotential height observed from 2 (top) to 9 (bottom) February 2018 over a domain (20° N–70° N). The thick contour corresponds to 10250 m. (b) ERA-I 250 hPa meridional velocity squared, contour intervals are 800 m² s⁻². The coloured lines track the movement of the ridges and troughs (a) and corresponding maximums of meridional velocity squared (b) and suggest the propagation of wave packets.

715

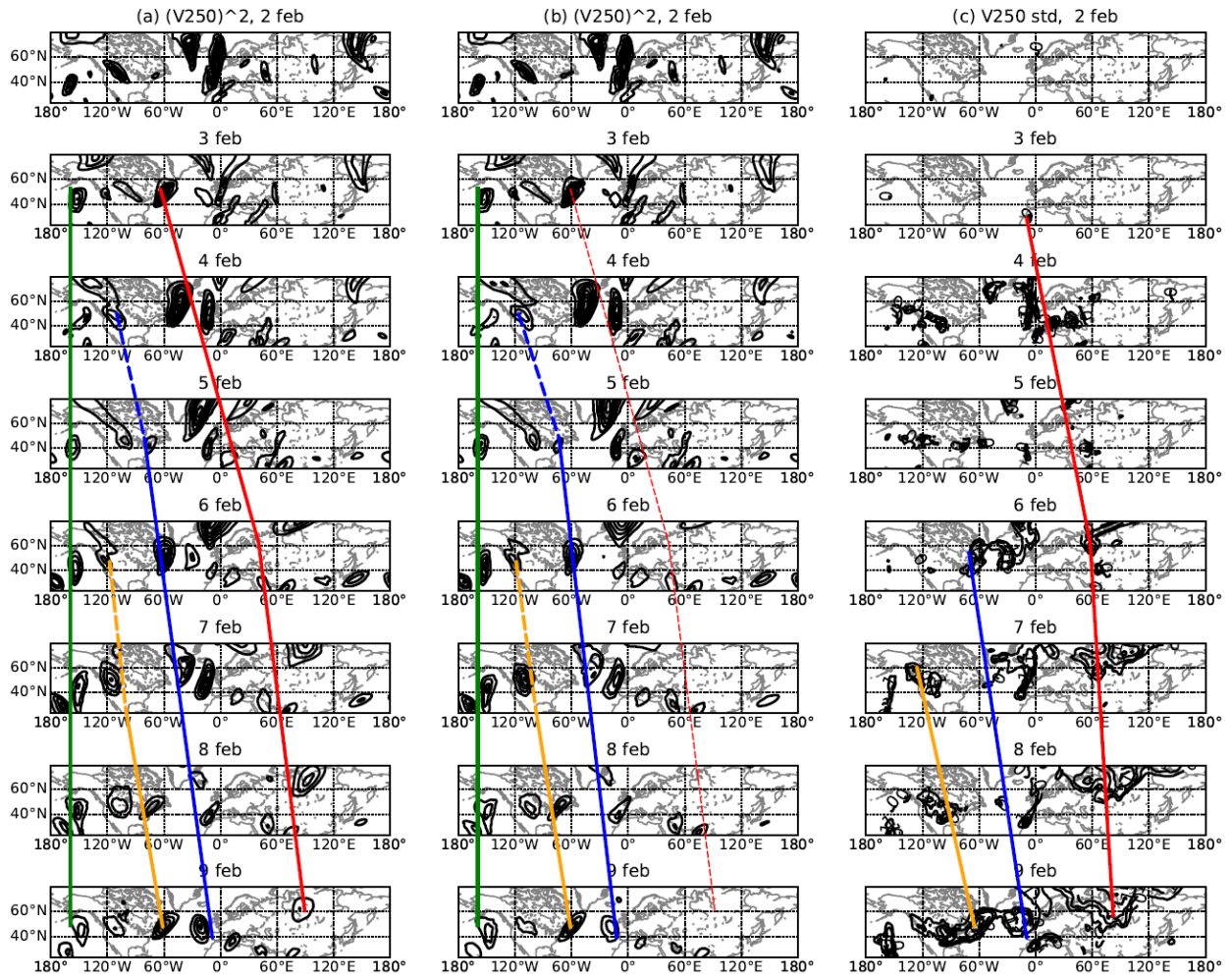


Figure 10. Same as Fig. 98b, but for ENS+ (a) and ENS- (b) members, contour intervals are $800 \text{ m}^2 \text{ s}^{-2}$. The red rectangles denote the wave train discussed in text. (c) standard deviation of the predicted 250 hPa meridional wind velocity among ensemble members. The standard deviation is normalized by the maximum and minimum within the domain. Contour intervals are 0.1 starting from 0.5. The coloured lines are mostly similar to those in Figure 9 and suggest the propagation of wave packets. The red line in Figure 10b is dashed to emphasize the lack of this wave train in ENS-. The green line in Figure 10c is missing because there is little forecast spread in the eastern Pacific.

720

725

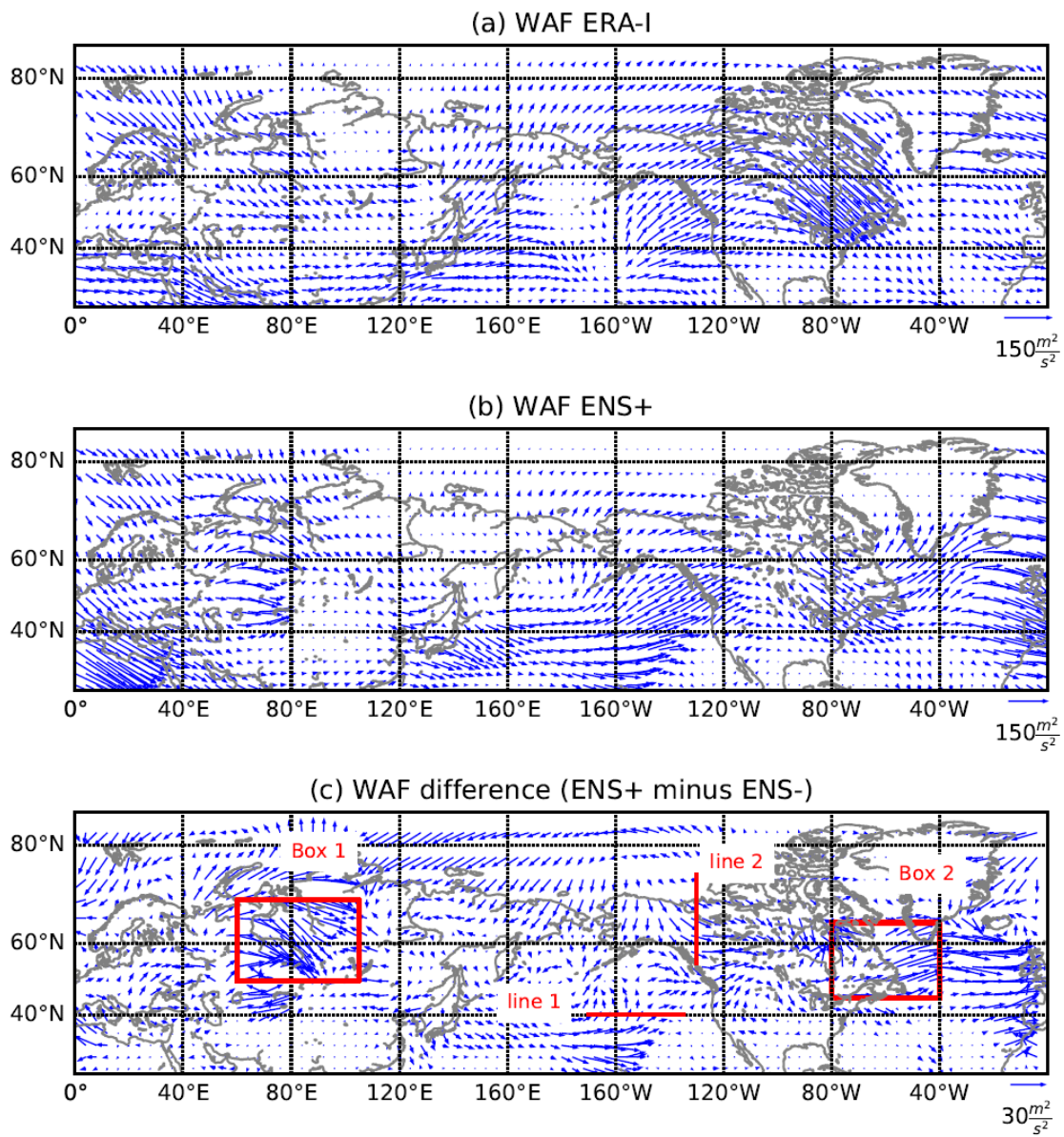


Figure 11. The 500 hPa horizontal WAF ($m^2 s^{-2}$) averaged over 5–7 February. (a) ERA-Interim;

730 (b) ENS+; (c) difference between ENS+ and ENS- groups of ensemble members.

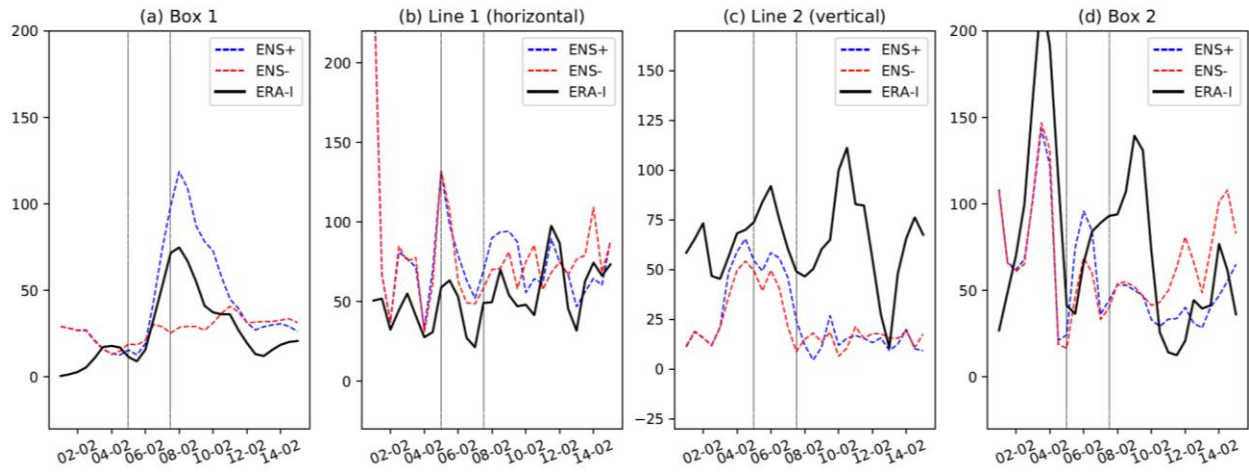


Figure 12. Time series of the horizontal WAF at 500 hPa ($\text{m}^2 \text{s}^{-2}$) averaged over the Boxes 1 and 2 and through the Lines 1 and 2 shown in Fig. 11**c**. (a) and (d) show mean length of the horizontal WAF vector while (b) and (c) show mean meridional and zonal components respectively. Grey vertical lines denote the averaging period taken for analysis in Fig. 11: 5 and 7 February.

735

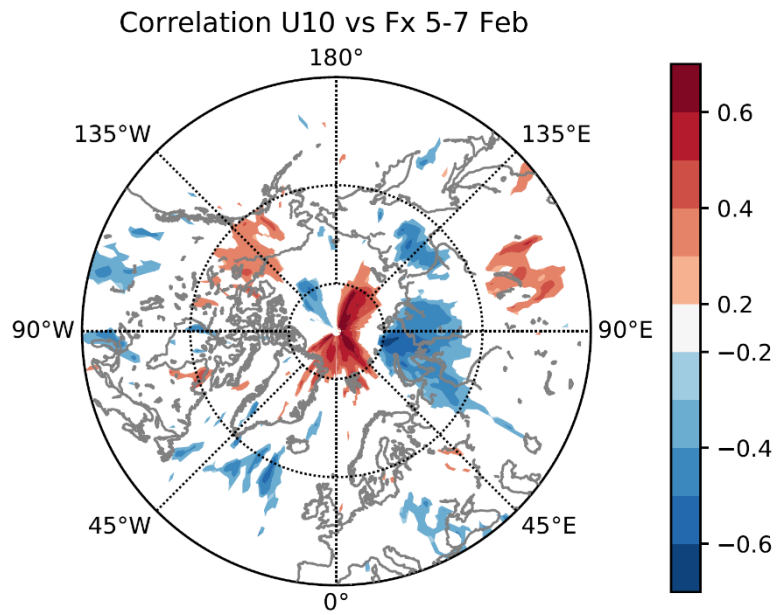
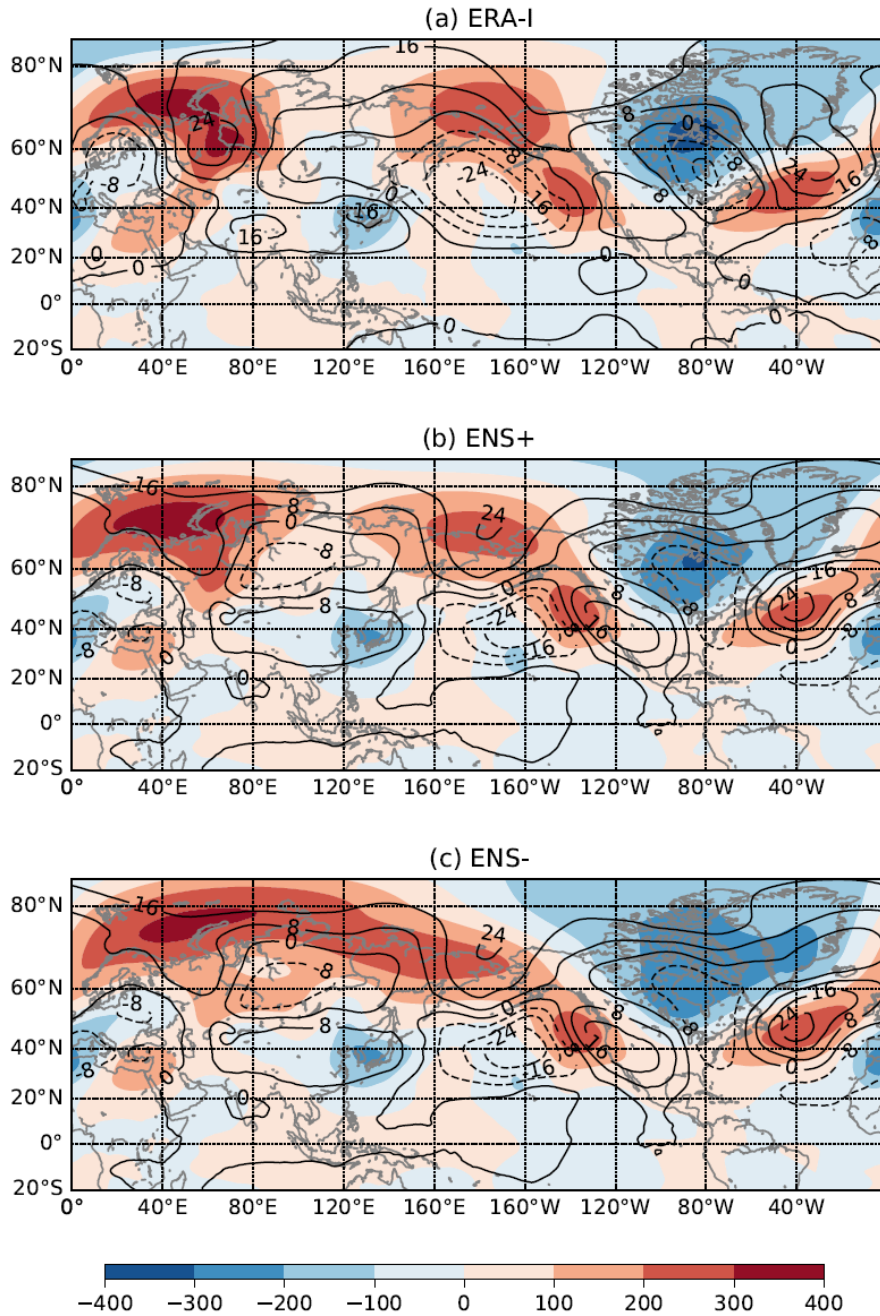
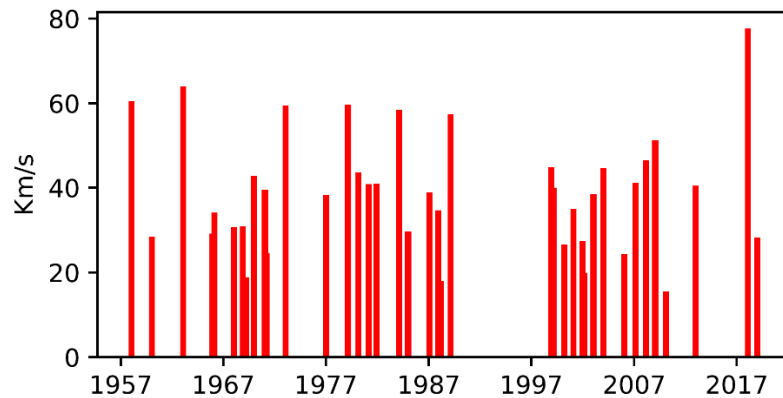


Figure 13. Correlation coefficient between zonal WAF at 500 hPa averaged 5–7 February and
740 U10 reanalysis on 12 February across individual ensemble members. All shaded coefficients are
significant at $p = 0.05$.

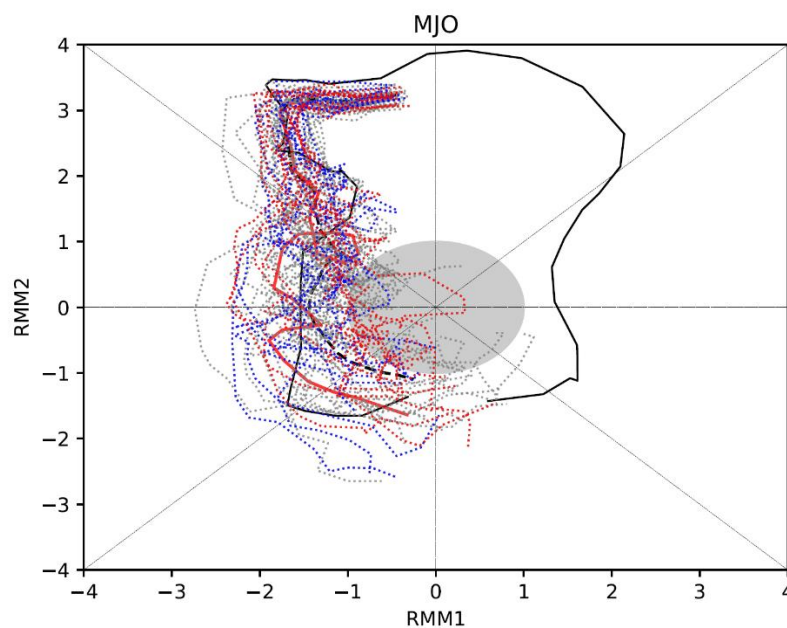


745 **Figure 14.** Geopotential height anomalies at 500 hPa in (a) ERA-I; (b) ENS+ members and (c)
ENS- members. Contours show Composite anomalies of geopotential height composite (m) for
picked only for days with MJO phase 6 with averaged over lags averaged lag of 5-9 days at 500 hPa
(contours) and anomalies of geopotential height at the same level averaged over 5-7 February
(shaded). Shading shows anomalies averaged over 5-7 February 2018. (a)-ERA-I, composites are
calculated using 1980-2010 data, (b) ENS+ members, composites calculated using hindcasts over 20
750 years (1997-2017), (c) same as in (b) for ENS- members. Forecast model composites are calculated
using hindcasts over 1997-2017.

Appendix A



755 **Figure A1.** Eddy heat flux at 100 hPa (Km s^{-1}) averaged across $50\text{--}75^\circ \text{N}$ observed over 5 days prior to a major SSW during 1958–2018. The dates of the SSWs are taken from Charlton and Polvani (2007) and Karpechko (2018). The heat flux in 1979–2018 was calculated using ERA-I reanalysis while in 1958–1978 – using ERA-40 reanalysis (Uppala et al., 2005).



760 **Figure A2.** MJO phase diagram. ECMWF 46-day ensemble forecast initialized on 1 February: blue dashed lines denote ENS+ members, red dashed lines – ENS– members, grey lines – all other members ([data source: http://s2sprediction.net/](http://s2sprediction.net/)). Red line denotes the control forecast, black dashed line – ensemble mean. [Forecast data is plotted for 1–28 February](#). Black solid line denotes RMM indexes from Bureau of Meteorology [between 15 January and 28 February 2018](http://www.bom.gov.au/climate/mjo/) (data source: <http://www.bom.gov.au/climate/mjo/>).

765